

Non-Linear Control for Floating Wind Turbines

Using Reset Control to overcome non-minimum phase zeroes

J.A. Berens

Master of Science Thesis

Non-Linear Control for Floating Wind Turbines

Using Reset Control to overcome non-minimum phase zeroes

MASTER OF SCIENCE THESIS

For the degree of Master of Science in Systems and Control at Delft
University of Technology

J.A. Berens

July 10, 2020

Faculty of Mechanical, Maritime and Materials Engineering (3mE) · Delft University of
Technology



Copyright © Delft Center for Systems and Control (DCSC)
All rights reserved.



Abstract

As the world is shifting away from fossil fuel-based electricity production, mainly due to concerns for man-made climate change, a sharp rise in demand for wind powered electricity production is seen. In order to meet future demand, the vast amount of off-shore wind resources can be unlocked. A key technology for this task are floating wind turbines (FWTs), as they are less constrained by water depth than fixed wind turbines. One challenge for FWTs is sometimes referred to as ‘negative aerodynamic damping’: interaction between the blade pitch controllers and the fore-aft motions of the floating platform (pitch and surge) can cause instabilities leading to large oscillations in platform motion and rotor speed. These interactions translate to right half-plane (RHP) zeros, limiting the system bandwidth and thereby the performance of the wind turbine. This increases the variability in the power output of the FWT. This thesis looks into a promising type of non-linear control to overcome this limit: reset control. Reset control is characterized by a higher phase compared to linear controllers. This could be used to improve the stability margins of the system and/or to increase the bandwidth. This thesis designs a CgLp controller specifically [1]. Using the CgLp, a theoretical improvement is seen in the frequency domain. Therefore, a better performance is expected. However, after time domain simulations, it is shown that this controller is not fit for application in blade pitch control. Two different configurations of the CgLp are considered. In the default configuration, large peaks are present in the control signal, leading to excessive motions of the blades. The second configuration performs well under idealized circumstances, but with high frequency disturbance (such as turbulent wind or sensor noise), excessive amounts of resets prevent the controller from reacting appropriately.

Table of Contents

Acknowledgements	xi
1 Introduction	1
1-1 Related research	2
1-2 Problem statement & research objective	3
1-3 Outline	4
2 Background Information	5
2-1 Basics of fixed bottom wind turbines	5
2-1-1 Fundamental principles of wind energy	5
2-1-2 Modeling and Control	6
2-2 Floating Wind Turbines	8
2-2-1 Platform Designs	10
2-3 Control of FWTs	12
2-3-1 Related studies	13
2-3-2	16
2-4 DTU 10MW Reference Turbine with SWE Triple Spar platform	18
2-5 Reset Control	19
2-5-1 Origins	19
2-5-2 Characteristics of reset control	21
2-5-3 State-Of-The-Art in Reset Control	22
3 Controller Design	31
3-1 Linear model	31
3-1-1 Linear baseline controller	32
3-2 Controller selection	33
3-3 Tuning	35

4 Results	45
4-1 Simulation cases	45
4-2 Linear Model	46
4-3 Non-linear simulations in FAST	53
5 Conclusion	57
5-1 Sub-objectives	57
6 Discussion and Recommendations	61
A Linearized Model	63
Bibliography	65
Glossary	71
List of Acronyms	71
List of Symbols	72

List of Figures

2-1	Torque-Rotor speed curve for a variable speed wind turbine [2]. The dotted lines show the curves for a wind turbine with fixed wind speed.	7
2-2	offshore wind turbines with seabed foundations [3].	9
2-3	Possibly the first FWT concept [4]. It features a spar buoy type floater with a single mooring line, and remarkably has three rotors, distinguishing itself from modern designs.	10
2-4	Three possible designs for a floating wind turbine [5]. These designs illustrate the different types of stabilization, but real platforms often rely on a combination of these mechanisms.	11
2-5	A semi submersible type floating wind turbine [6]. Based on the offshore experience of the petroleum industry, this design combines the mechanisms for stability. . .	12
2-6	Minimum thrust operation strategy. The black line is the regular constant speed controller, the red line is the minimum thrust strategy. [7]	14
2-7	Robust gain scheduling compared with gain scheduling for a regular wind turbine and detuned gains of a floating wind turbine. [8]	14
2-8	Parallel path modification. The feedback loop is applied to modify the wind turbine system. [9]	15
2-9	Initial undershoot caused by a RHP zero. The system is defined as: $G(s) = \frac{-s+1}{s^2+2s+1}$	16
2-10	Bode plot comparing systems containing a RHP zero and a LHP zero. The gain behavior is exactly the same, but the RHP zero's phase decreases.	17
2-11	Diagram of closed loop reset control for a FWT. The shifted rectangle represents a reset controller. The signals: $r(t)$ is the reference, in this case the rated rotor speed. $e(t)$ is error signal. $u(t)$ is the blade pitch angle. $d(t)$ is the disturbance, in this case the wind speed. $y(t)$, the output, is the measured rotor speed.	19
2-12	Output of the Clegg Integrator with sinusoidal input, compared to a regular integrator.	20
2-13	Output of the FORE (solid) with sinusoidal input (dashed) [10]	21
2-14	A Clegg integrator (CI) in a feedback loop leading to Zeno solutions. After each reset the time until the next reset decreases. [10]	22

2-15	PI+CI controller structure. The parallel connection means that only part of the controller state is reset, defined by the reset percentage (the ratio of the linear and CI integrator gains) [11]	23
2-16	Response to a sinusoidal input of a FORE with reset band. The dotted line is the error, the solid line is the controller's output. [12]	24
2-17	Phase of the FORE with reset band, depending on the relative size of the reset band $\frac{\delta}{E}$. [12]	24
2-18	Time domain response of the HIGS. For the red segments, the response is like that of an integrator. For the green segments, it is a proportional gain. Note that when switching modes, the state is saved [13].	27
2-19	Describing function of the HIGS for changing parameters [14]	28
2-20	Describing function of the CgLp [1]	29
3-1	Bode plot from blade pitch to rotor speed of the linearized DTU 10MW with SWE triple spar platform at a wind speed of 12 m/s, derived using simplified low order wind turbine (SLOW) [15].	32
3-2	Bode plot of the linearized floating wind turbine at 12 m/s with the linear PI controller. It is shown in the figure that at the point where the system's phase crosses -180 degrees, the integrator of the PI is barely active anymore, leaving little room for improvement there.	34
3-3	Bode plot with a comparison between a linear PID (as in Equation 3-5) and a PID with a CgLp, based on its describing function.	36
3-4	Bode plot of the describing function of the CgLp. Phase peaks at 32.2 degrees at 0.25 radians per second. At the desired bandwidth of 0.127 radians per second, the phase is 25 degrees.	37
3-5	Bode plot of the describing function of the controller with CgLp (blue) and the linear baseline controller including the low pass filter (orange). The magnitude and phase lines cross over at the open loop crossover frequency, leading to the same bandwidth and phase margin. However, improved tracking performance and attenuation are shown, as well as a higher gain margin.	38
3-6	Bode plot showing stability margins for the open loop with CgLp. The bandwidth and phase margin are the same as the base linear system, but the gain margin has improved.	38
3-7	Bode plot comparing the open loop of the controller with CgLp to the linear baseline. Significant improvement is expected at low frequencies, especially the zeros at 0.034 rad/s corresponding to the surge motions of the platform. Also, a slightly better high frequency roll-off is seen.	39
3-8	These graphs show the linearized wind turbine's response to a step in the wind-speed. The blade pitch is shown on the left, and the rotor speed on the right. This figure shows the CgLp in both configurations as well as the linear baseline. Large peaks are shown in the blade pitch signal for method 1, over ten times as large as with the other method. Also, oscillations at the fore-aft tower bending mode's natural frequency show up in the rotor speed signal.	40
3-9	These graphs show the linearized wind turbine's response to a step in the wind-speed. The blade pitch is shown on the left, and the rotor speed on the right. The graph shows the base linear system in orange and the CgLp in blue, where the order is like in method 2 (Lead Filter - SORE).	41
3-10	Bode plot of the second controller compared to the linear baseline.	42
3-11	Open loop bode plot of the second controller with the FWT	42

3-12	These graphs show the linearized wind turbine's response to a step in the wind-speed. The blade pitch is shown on the left, and the rotor speed on the right. The graph shows the base linear system in orange and the CgLp in blue	43
4-1	This figure shows an extended version of the simulations from the previous chapter with the first (slower) CgLp. It shows the FWTs behavior after a 1 m/s step on the wind speed. After the CgLp initially excited more oscillations at the platform pitch natural frequency, it shows a better rejection of the low frequency disturbance due to surge motions. This matches the frequency domain, where we see a higher gain at the zero pair corresponding to the surge motion.	47
4-2	This figure shows an extended version of the simulations from the previous chapter with the second (faster) CgLp. It shows the FWTs behavior after a 1 m/s step on the wind speed. The frequency domain expectations do not hold here, as no improvement is seen because the oscillations at the platform pitch frequency continue throughout the simulation.	47
4-3	This figure shows the behavior of the linearized FWT model under turbulent wind. Clearly, the CgLp performs much worse, as there is much more variation in the rotor speed. The blade pitch does not seem to respond well compared to the linear baseline.	48
4-4	This figure shows the first 50 seconds of the simulation in Fig 4-3.	48
4-5	The filtered wind speed signal. A lowpass filter with corner frequency $\omega = 0.5$ rad/s is used. The signal is averaged at zero so that it can be used for the linearized model.	49
4-6	Simulation with filtered wind signal. The graph shows that the CgLp performance is quite similar to the linear performance. At some times, it clearly takes advantage of the phase lead over the linear controller, while at other times, the resets seem to delay the performance.	49
4-7	Simulation with filtered wind signal. While the blade pitch signals seem quite similar, the derivative (pitching speed) tells a different story. Large peaks are shown for the CgLp, so the pitch motors are working very rapidly.	50
4-8	Step response with an increased loop gain by 60%. The linear baseline is barely stable, but the CgLp shows similar behavior to the normal gains. For this design, the gain margin is 0.23 dB and the phase margin is 5.35 degrees. Therefore, the response dampens out much quicker than expected.	51
4-9	The simulation from Figure 4-8, zoomed in on the first 80 seconds.	52
4-10	Simulation of Two CgLp's with the FWT, where one has the loop gain increased by 3%. This increased gain actually seems to make the performance slower due to a badly timed reset.	52
4-11	Simulation with FAST of a step in the wind, (from 11.5 to 12.5 m/s) with the CgLp and the linear baseline controller. A reset is also shown when the blade pitch was still rising towards the value it settles at, making its performance worse compared to the linear baseline.	53
4-12	Simulation with FAST with turbulent wind, (averaged at 12 m/s) with the CgLp and the linear baseline controller. Excessive resets can be seen in the blade pitch signal of the CgLp.	54
4-13	Simulation with FAST of a step in the wind, (from 11.5 to 12.5 m/s) with the CgLp and the CgLp with filter. An improvement is shown because the filtered CgLp avoids resetting too soon. A similar overshoot as the linear baseline can be seen, and the phase advantage of the CgLp still shows (the oscillations are shifted to the left compared to the linear baseline.)	55

-
- 4-14 Simulation with FAST of turbulent wind (averaged at 12 m/s) with the CgLp with filter compared to the Linear baseline. The CgLp's performance is much better with a filtered rotor speed signal. However, it still does not perform as well as the linear controller. The RMS error of the CgLp is 0.71 rpm, while the RMS error of the linear baseline is 0.59 rpm. 55

List of Tables

4-1	root mean square (RMS) error for the CgLp and linear baseline controller in simulations with Normal Turbulence Model (NTM) and the filtered wind speed. The CgLp performs better than the linear controller when the wind input does not contain high frequencies.	50
-----	--	----

Acknowledgements

Firstly, I want to thank my supervisors, prof.dr.ir. J.W. van Wingerden and dr.ir. S. Mulders for their advice and guidance.

Secondly, many thanks to the committee members, dr.ir. H.S. HosseinNia and ir. J.A. Frederik for taking the time to read and scrutinize my work.

Last but not least, my gratitude goes out to anyone who has supported me and expressed their belief in me. Friends, family and my girlfriend enabled me to complete this work.

Delft, University of Technology
July 10, 2020

J.A. Berens

Chapter 1

Introduction

Man made climate change has the potential to disrupt life on earth as we know it [16]. Almost all the countries of the world have pledged their cooperation to mitigate greenhouse gas emissions, in order to avoid warming of the global average temperature further than two degrees Celsius. A steep decrease in use of fossil fuels is demanded, which creates a great demand for alternative forms of energy. Besides man made climate change, other reasons for shifting away from fossil fuels exist. Firstly, burning of fossil fuels is associated with air pollution. Secondly, most countries now depend on few foreign nations for their energy supply. Therefore, a shift to renewable energy can make their economies independent from foreign supplies. Due to these concerns, the demand for renewable energies in general, and wind energy specifically, has risen. In [17], it is shown that land-based wind turbines, excluding forests, urban areas and land ice, can supply the world's electricity demand 40 times over, (or five times the final energy consumption, including heat and fuels).

However, many reasons exist to opt for offshore wind turbines instead of land based wind turbines. First of all, land based turbines face political opposition. In [18], different types of concerns of people opposing wind turbines are named, such as aesthetics, noise, financial, and environmental concerns. Furthermore, wind is known to be stronger and more constant at open sea. Thirdly, demand in densely populated countries exceeds availability of suitable areas for wind turbines on land.

The installed capacity of offshore wind turbines has been steadily rising this decade [19]. As the paper shows, almost all of these wind turbines have fixed foundations in the seabed, with the most common type being a monopile. Another type of substructure listed in the paper, the floating platform, has been the subject of many recent studies [20]. Floating wind turbines (FWT s) offer many advantages over fixed offshore wind turbines, but they pose challenges too [21].

One of the reasons for choosing an floating wind turbine (FWT) over a fixed offshore wind turbine is that they can be placed on the surface of deeper bodies of water [22]. Secondly, they can be constructed in a dock and towed to the desired location, so construction is safer and cheaper compared to a fixed turbine, that needs to be built on sea. Because of this, sea

life is not disturbed as much by construction of floating wind turbines [21]. Hypothetically, a floating wind turbine can even be towed towards the coast for safer maintenance.

Several different designs for an FWT have been proposed, based on different kinds of buoyant parts and anchoring. These different designs will be addressed in chapter 2.

While FWTs could unlock a vast volume of wind resources, they still pose various challenges to engineers. The main challenge that is addressed by this thesis is the coupling between platform motions and rotor speed. The floating platform can pitch (rotating rigid body mode) and surge (translating rigid body mode), leading to much bigger fore-aft motions of the tower compared to a fixed wind turbine. These motions cause an induced wind at the rotor. This oscillating induced wind, coupled with blade pitch control, can lead to an unstable loop, exacerbating these rigid body motions. Therefore, for a classical pitch controller, the system bandwidth is limited at the natural frequency of this motion.

Different control methods have been proposed to deal with this resonance, all with different advantages and disadvantages. These methods are quickly reviewed in chapter 2. While some methods lead to a greatly reduced performance compared to fixed wind turbines, others perform better at the cost of an increased complexity. An improved control method that is not overly complex can increase feasibility for FWTs [5].

One promising control technology is reset control. Reset control is a type of non-linear control, that was first introduced by J.C. Clegg, who designed the Clegg Integrator in 1958 [23]. The Clegg Integrator (CI) shares most of its characteristics with a linear integrator, with the advantage of a lower phase loss. Instead of a 90 degree phase loss, the describing function of the CI shows a 38 degree phase loss. This leads to increased stability margins and can allow for a higher system bandwidth.

These advantages of reset control, paired with the fact that it can be implemented like a regular integrator in a simple single input single output (SISO) control loop, make it an interesting candidate to research.

1-1 Related research

In the field of floating wind turbine control, the main problem is referred to as 'negative aerodynamic dampening' [7]. In control engineering terms, this problem is defined by a right half-plane zero (RHPZ). The RHPZ destabilizes the system if the controller gains for the blade pitch controller are too high. Further explanation on this dynamic is given in Chapter 2.

The most simple way to avoid instability in FWTs is decreasing the gains. In [7], a systematic approach is given to design a controller for an FWT with reduced gains. While the loop is stabilized, it leads to a lowered bandwidth, which causes larger overshoot of the rotor speed. An improvement can be made by adjusting the way that the controller gains are scheduled, to achieve the same stability margins [8] at each operating point. The dynamics are not critical for every wind speed, so gain scheduling can account for this, increasing the gains for less critical (higher) wind speeds.

Another approach is found in [24], where the induced wind due to platform pitch motions is estimated based on measurements of the platform pitch. This information is used to

compensate for variations in rotor speed. It shows promising performance for idealized wind conditions, but no results have been achieved in realistic wind conditions.

A different way to tune the controller for FWTs is discussed in [25]. In the above rated region, instead of controlling for constant rotor speed (and constant generator torque), the controller aims to operate with minimum rotor thrust, while still generating the rated power. This is achieved by reducing the tip-speed ratio λ . The wind turbine operates at a lower rotor speed, with a higher torque. The blades are pitched further compared to a regular controller. While it shows an improved behavior for power production compared to a normal detuned controller, the increased generator torque puts higher loading on the drivetrain and increases side-to-side motions.

MIMO control Many experimental controllers are based on using more control variables or measuring different system states, leading to multiple input multiple output (MIMO) controllers. An example is [9], where a second SISO loop is added to modify the system behavior for the blade pitch to rotor speed loop. This secondary loop is based on measured tower top movements and controls the generator torque. When this loop is active, the system is modified so that it does not have a RHPZ anymore, and therefore the bandwidth can increase. However, the method is still limited. A high gain for the inner loop might be necessary to achieve this improvement, which increases variations in the generator torque and thereby current. The generator must be designed for this purpose [15]. Note that this is not strictly MIMO control, however it is still included because additional variables must be measured and controlled.

Another MIMO strategy is the model predictive controller (MPC) discussed in [26]. In MPC, optimal control actions are continuously selected based on measured variables and a model of the system. While the study shows promising results, model based control is not popular in the industry as it relies on a simplified model of the wind turbine. Therefore, unmodeled dynamics can influence its robustness. However, as [27] notes, MPC is especially suited to operate with disturbance information. Wind turbines can be equipped with Light Detection and Ranging (LIDAR) systems [28] to measure the incoming wind. This information can be used in the MPC. However, using a LIDAR system is possibly not cost effective.

In summary, many approaches for dealing with the negative aerodynamic dampening can be found in the literature. While they all offer a solution for the problem at hand, a trade-off is always present. It is unlikely that a perfect solution exists, but it is still worthwhile to look into alternatives. This thesis will look into reset control as an alternative. Reset control offers the possibility to increase the phase of a system, allowing for a higher bandwidth with similar stability margins. It could achieve this while letting the control loop otherwise unaltered: no other variables have to be measured or controlled.

1-2 Problem statement & research objective

While FWTs are very attractive because of the advantages discussed earlier, their control performance is still heavily limited due to the RHPZ. Different options to solve it have been visited, but those also have downsides. Reset control seems promising from a theoretical standpoint, with the possibility to improve the phase loss of a controller. Some practical

implementations are also promising, however no research has been done on reset control for FWT control or another system with a RHPZ. This leads to the main research question:

Investigate possibilities to increase the control performance of FWTs based on advanced reset controllers

To help achieve this research goal, sub-objectives are defined. First of all, theoretical background information is given in Chapter 2, both on FWTs and on reset control. This information must be distilled into a choice for a controller structure. Together with a model of a FWT, the full system can be tuned.

Deliberately select a controller architecture that is most suitable for implementation with FWT and tune it for a specific FWT model

To answer the main question, an analysis must be made. Different types of simulations should be made to evaluate the performance of the controller, exposing any remarkable behaviors that might be relevant. Based on these results, conclusions can be drawn about the possibilities to increase control performance.

Perform simulations comparing the reset based controller to a baseline controller, to review the performance of reset control for FWT

Here, performance is primarily defined by the variations in the rotor speed. The blade pitch speed must be taken into account as well, as it can expose a trade-off.

1-3 Outline

This thesis is divided into 5 chapters, this introduction being the first one. The second chapter gives the necessary background information needed to put the research into context. Also, a model of a FWT is introduced that will be used throughout the thesis. In Chapter 3, the design process for a reset based controller for this FWT is described. This includes choosing the most suitable type of controller and tuning it. In Chapter 4, simulations of the FWT are shown, both with the designed reset controller and a baseline controller for comparison. In Chapter 5, the results are analyzed, drawing conclusions from the simulations. This includes insights into the characteristics for reset control and its suitability for control of FWTs. Chapter 6 discusses the thesis and gives recommendations for future research.

Background Information

In this chapter, all the relevant background information about floating wind turbines (FWTs) and reset control is given. To deeply understand the difficulties of floating wind turbines, it is important to start with a good understanding of a regular (fixed bottom) wind turbine. After that, turbines on a floating platform are considered. A specific wind turbine model is introduced that will be studied in this thesis. Lastly, an introduction in reset control is given. An overview of the research field is given, providing the necessary information to design a reset controller for a floating wind turbine.

2-1 Basics of fixed bottom wind turbines

Firstly, the physics behind extracting energy from wind will be discussed. Then, a brief review of the mechanical and electrical parts of the wind turbine is done. Lastly, this chapter gets into the basics of wind turbine control.

2-1-1 Fundamental principles of wind energy

Wind turbines extract kinetic energy from the wind. To achieve this, the wind must be slowed down. If the wind speed flowing into the rotor is V_1 , and behind the rotor V_2 , the wind speed in the rotor plane is assumed to be $V = (V_1 + V_2)/2$. Then, the mass flowing through the rotor's area is: $\dot{M} = \rho V \pi r^2$. ρ is the air density, r is the rotor's radius. The power extracted by the rotor, following Newton's second law, is defined by:

$$P = \frac{1}{2} \dot{M} (V_1^2 - V_2^2) = \frac{1}{4} \rho (V_1^2 - V_2^2) (V_1 + V_2) \pi r^2. \quad (2-1)$$

The total available wind power is given by $P_0 = \frac{1}{2} \rho V_1^3 \pi r$. Then, the power factor, is given by

$$C_p = \frac{P}{P_0} = \frac{1}{2} \left(1 - \left(\frac{V_2}{V_1}\right)^2\right) \left(1 + \left(\frac{V_2}{V_1}\right)\right). \quad (2-2)$$

The optimum of this function is found at $V_2/V_1 = 1/3$. This gives $C_p = \frac{1}{2} \times \frac{8}{9} \times \frac{4}{3} = \frac{16}{27}$. This power factor of $C_p = \frac{16}{27} \approx 59.3\%$ is known as the Betz limit, and is the theoretical maximum efficiency of any machine that extracts power from the wind.

A real machine will not be able to reach this limit as inefficiencies exist, for example in the gear box, the generator, and the converter [29]. To maximize the power factor, modern wind turbines are generally variable speed wind turbines [30]. As the maximum power factor occurs at a fixed tip speed ratio, the rotor speed must be proportional to the wind speed (which is obviously variable too). The tip speed ratio (TSR), λ is the ratio between the wind speed and the speed of the blade tips of the wind turbine. Essentially, this defines the inflow angle for each blade.

However, wind turbines are designed with a rated power. This is the maximum power that the generator can sustain. If the power that the machine extracts from the wind exceeds this value, the C_p should decrease to avoid damaging the generator. This can be achieved by adjusting the blade pitch angle. This is called the **above rated** region, and the region where C_p is maximized through variable speed operation is called **below rated**.

In general, the rated power of a wind turbine is decided first, and a generator is selected. The rotor size is selected afterwards, based on average wind conditions at the chosen site. Many wind turbines come with different rotor sizes, aimed at different locations with varying wind speeds. If a very big rotor size is chosen, the wind turbine reaches its rated power at a lower wind speed and therefore it spins at its rated power more often. This approach yields a high capacity factor, but it is more expensive. Above the rated power, the wind turbine can not absorb all the energy in the wind and must therefore pitch its blades. So while a big rotor can reach a high capacity factor, it is not always very efficient economically. If a smaller rotor size is chosen, the generator will run at its peak power less often. This option is more attractive in areas with constant high winds. Other factors are fixed costs for the wind turbine (such as grid connection and ground). If these costs are very high, its more attractive to aim for a high capacity factor.

2-1-2 Modeling and Control

As discussed earlier, a variable speed wind turbine can operate in different regions: Below or above the rated wind speed. Some extra stages can be defined by the transitions (start up, shut down and a transition between below and above rated), as seen in Figure 2-1.

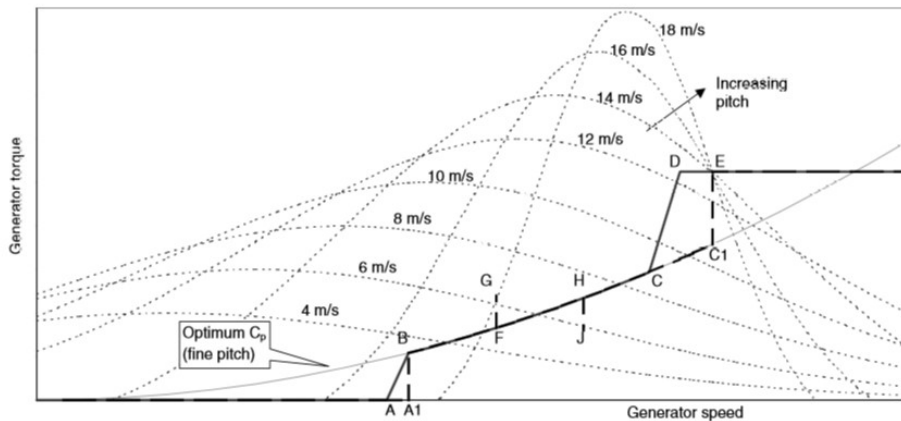


Figure 2-1: Torque-Rotor speed curve for a variable speed wind turbine [2]. The dotted lines show the curves for a wind turbine with fixed wind speed.

Below rated Below the rated wind speed, (region B-C in figure 2-1) the turbine is exploiting its peak power potential. Therefore, it would be ideal to reach the wind turbine's highest possible power factor. Since this happens at a fixed TSR, the rotor speed should be proportional to the wind speed. The torque controller can vary the generator torque to achieve this optimal rotor speed. To achieve this, the torque should be proportional to the wind speed squared. As discussed before, the rotor speed should be proportional to the wind speed, and since it is more difficult to estimate the wind speed, this can be used as an input for the torque controller. The following rule can be used [2]:

$$T = K\omega_g^2 \quad (2-3)$$

$$K = \frac{\pi\rho R^5 C_p}{2\lambda^3 G^3} \quad (2-4)$$

Above rated When the wind turbine operates at wind speeds greater than its rated speed, it must reduce the power factor C_p . Point E in Figure 2-1 marks the rated power, and at this point, the rotor speed and rotor torque should remain constant. To achieve this, the wind turbines blades are pitched into a less optimal position. This is shown in Figure 2-1, where all the dotted curves for higher wind speeds pass through the point E. The angle attack for the blade is either increased or decreased to achieve this. This referred to as pitching to stall or pitching to feather. A feedback loop is used to control the pitch angle, in general, a PID controller:

$$PID = K_p + \frac{K_i}{s} + \frac{K_d s}{1 + s\tau} \quad (2-5)$$

In addition to the PID controller, filters can be used to dampen out undesirable system modes. In order to tune the controller, it is useful to use frequency domain design tools. However, due to the very non-linear nature of a wind turbine, linearized models needs to

be used for controller design. A very large part of the non-linearity is due to the non-linear relationship between the aerodynamic torque and the blade pitch: the same change in blade pitch will not always yield the same change in aerodynamic torque. [31]. It has been shown that linearizations at different operating points generally only differ in gain, not in shape. Therefore, the easiest way to deal with this non-linearity is to include a gain scheduling factor for each operating point. The full gain-scheduled PID controller consists of a nominal PID controller designed for one operating point, and a polynomial defining the gain scheduling factor for the other operating points.

Reducing loads Both blade pitch control and generator torque control can be used to reduce the loads on the system [32]. Firstly, while designing the control algorithms for regular operation, it is important to take into account the controller's effects on loading. For example, the bandwidth should be chosen with resonance modes of the structure in mind. However, load reduction can also be an objective of its own. Torque control is used to account for resonance of the drivetrain. A sensor can be placed on the nacelle to detect fore-aft motions of the tower, allowing a feedback loop to be added for reduction of this motion using an additional signal to collective pitch control. Blade pitch can be controlled for each blade individually, to account for cyclic loads (for example due to aerodynamic effects of passing by the tower each rotation). As wind turbines increase in size, fatigue stress becomes more critical and these control strategies become increasingly important.

2-2 Floating Wind Turbines

As discussed in the introduction, offshore wind turbines are becoming increasingly popular. Many reasons to move wind turbines off shore exist, for example [33]:

- Decreasing amount of suitable sites on land
- Fewer constraints on turbine size
- Higher and more reliable wind speeds
- Increased demand for renewable energy

Currently, almost all offshore wind turbines have foundations in the seabed, with different designs depending on the water depth and soil, as shown in figure 2-2.

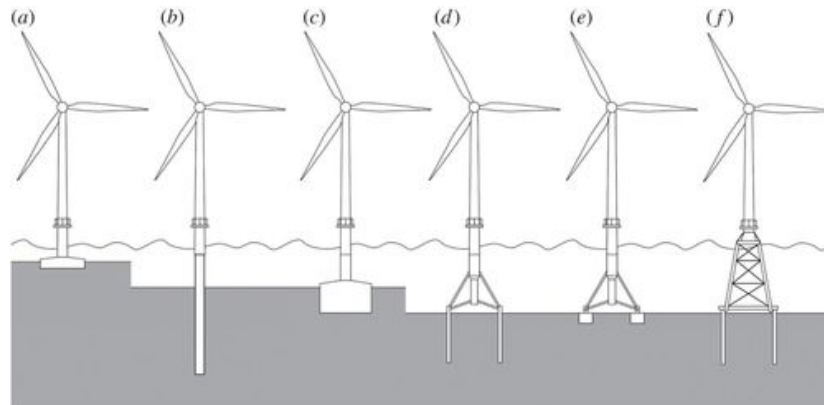


Figure 2-2: offshore wind turbines with seabed foundations [3].

These foundations are heavy and expensive, their construction disturbs sea life, they are difficult to access for maintenance, they require specialized vessels to build, and the maximum depth for economically viable fixed offshore turbines is limited [22]. All these disadvantages have inspired a lot of research into floating wind turbines. FWTs can offer solutions for these problems. For example, they can be built on land and towed towards their site, and are economically viable in much bigger depths.

Obviously, there are also challenges. First of all, there are many different floater designs, and selecting the most suitable one is not trivial. Additionally, the platform-turbine system has rigid body resonance modes that interfere with the blade pitch controller of a regularly tuned wind turbine [7].

The idea to build floating wind turbines is not new, as first concepts (see Figure 2-3) go as far back as 1972 [4]. The paper cites the risk associated with nuclear energy, as well as externalities not included in the cost of fossil fuel based plants, as a reason to turn to wind energy. The author goes over different concepts, including a floating turbine with 100 rotors and also a fixed bottom offshore wind turbine, and includes a way to store energy to account for the sources variability.

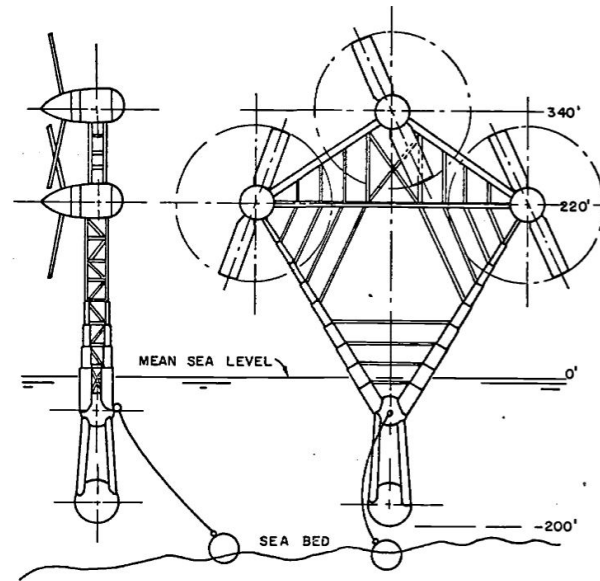


Figure 2-3: Possibly the first FWT concept [4]. It features a spar buoy type floater with a single mooring line, and remarkably has three rotors, distinguishing itself from modern designs.

Because of these engineering difficulties and high cost, it has only been in recent years that full scale prototypes of FWTs have been tested. The first full size floating wind turbine demo, Hywind, was realized in 2009 just offshore Norway's coast [34]. Since then, a 30 MW floating wind farm has started production in 2017 in the North sea near Scotland [35]. This wind farm is featured on the cover of this MSc thesis [36].

2-2-1 Platform Designs

In general, a floating wind turbine can be viewed as a regular wind turbine, placed on top of a floating platform. The platform provides buoyancy and stability. In other words, it makes the system stay afloat and upright. It is attached to the seafloor only with mooring lines. In this section, different types of platform and the effect they have on the system dynamics will be discussed.

The first requirement for the platform was to provide buoyancy. This means that, by Archimedes' law, the volume of the platform should be larger than the volume of the system's weight in water. Stabilization is more complicated however, and different approaches (shown in Figure 2-4) are researched:

- Ballast stabilization (spar buoy)
- Mooring line stabilization (tension leg platform)
- Buoyancy stabilization (barge)

For ballast stabilization, a perturbation in the pitch angle of the platform, will shift the center of gravity, leading to a restoring moment. Tension legs are stiff cables that pull the platform

down. As such, it is stabilized by the tension in these cables. The additional advantage is that the platform floats under the water surface, making it more resistant to waves. The stiff cables make the platform less susceptible to rotational rigid body modes. Buoyancy stabilization is based on the center of buoyancy shifting after a perturbation of the pitch angle, leading to a restoring moment.

Three designs based on these three methods of stabilization are shown in figure 2-4. All these designs lead to different characteristics, which makes it hard to optimize for the full system.

Other designs are possible too, which rely on a combination of these methods for stabilization. An example is a semi-submersible type platform, derived from oil rig designs. It derives stabilization from all three methods, while having most of the hull under the sea level. Therefore, the water plane area is smaller, making the platform less susceptible to waves. An example is the Dutch tri-floater, as seen in figure 2-5.

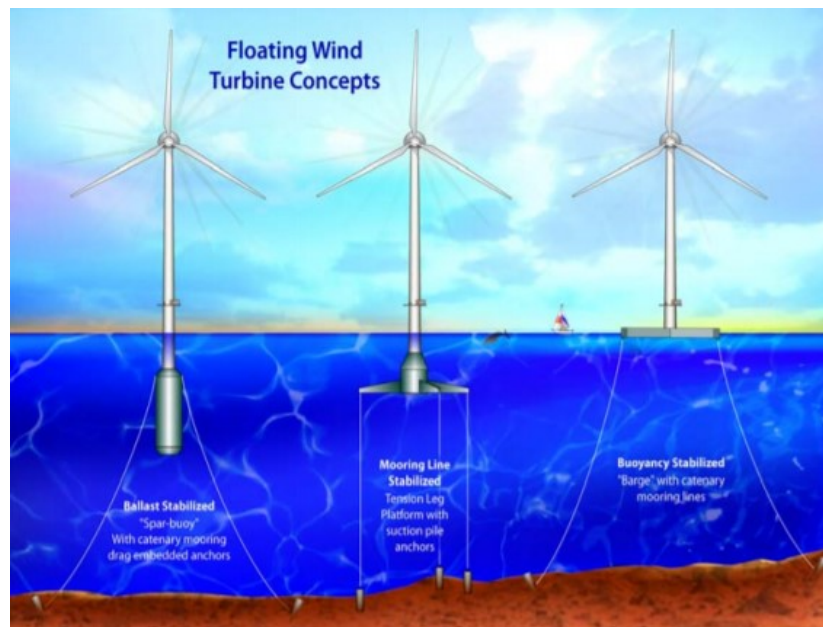


Figure 2-4: Three possible designs for a floating wind turbine [5]. These designs illustrate the different types of stabilization, but real platforms often rely on a combination of these mechanisms.



Figure 2-5: A semi submersible type floating wind turbine [6]. Based on the offshore experience of the petroleum industry, this design combines the mechanisms for stability.

2-3 Control of FWTs

Control of an FWT is very similar to control of a fixed bottom wind turbine. However, there is one important difference that makes controlling an FWT more challenging: rigid body modes. While a regular wind turbine can be modeled like a cantilever beam, the constraints at the base of an FWT are very complex and non-linear. This allows for rigid body modes, most importantly translation and rotation in the fore-aft direction (surge and pitch). These cyclical movements can lead to a positive feedback loop, for example with the rotational rigid body mode:

1. Wind Turbine pitches forward
2. Rotor experiences higher relative wind and speeds up
3. Controller pitches blades, leading to reduced thrust
4. The turbine pitches even further forward

And then, when the restoring moment of the platform overcomes this effect:

1. Wind Turbine pitches backwards

2. Rotor experiences lower relative wind and slows down
3. Controller pitches blades, leading to increased thrust
4. The turbine pitches even further backwards

This has been described as negative aerodynamic dampening [7]. Since the platform pitch isn't sufficiently dampened by other forces (hydrodynamic, mooring lines), this can lead to the wind turbine making larger and larger excursions each cycle, becoming unstable. In the real world this would likely be a (high magnitude) limit cycle, since the machine is non-linear. To counteract this, the pitch controller for a regular wind turbine should be detuned, making the blade pitch movements less aggressive. However, this leads to a lower bandwidth and thus worse system performance. For example, the rotational speed could overshoot the rated speed by larger amounts. This impacts the design of parts of the wind turbine that need to take this overshoot into account, possibly leading to higher costs.

For surge movements, the natural frequency is lower, potentially limiting the controller even further. However, this mode is sufficiently dampened by mooring lines and hydrodynamic forces [7].

2-3-1 Related studies

Attempts to dampen these motions have been made. This section will go over other studies that have addressed this problem.

Detune control gains The first solution to the instability of floating wind turbines is to simply use lower the controller gains. A systematic way of designing a detuned controller is presented in [7]. Results are compared to a land based wind turbine and a FWT with the same controller as the land based one. That FWT becomes unstable, and results show that the detuned controller solves this instability. However, overshoot of the rotor speed is significantly increased.

Another way to tune the controller differently for FWTs is discussed in [25]. In the above rated region, instead of controlling for constant rotor speed, the controller aims to operate with minimum rotor thrust, while still generating the rated power. This is achieved by reducing the tip-speed ratio λ . The wind turbine operates at a lower rotor speed, with a higher torque. The blades are pitched further compared to a regular controller. This operation strategy is shown in Figure 2-6.

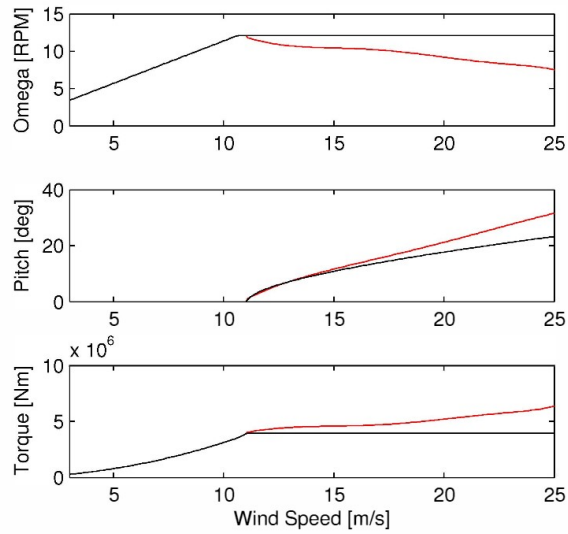


Figure 2-6: Minimum thrust operation strategy. The black line is the regular constant speed controller, the red line is the minimum thrust strategy. [7]

Gain scheduling can also be used to achieve better performance for a regular controller with detuned gains. For a fixed bottom wind turbine, the gains are scheduled to keep decreasing for higher wind speeds. However, in FWTs, stability is most critical close to the rated wind speed. Therefore, in contrast with a conventional wind turbine, a low controller gain is necessary at these lower wind speeds, and it can increase at higher wind speeds to achieve a higher bandwidth. In [8], a robust design method has been proposed to use gain scheduling to achieve the same stability margins at each wind speed. A comparison with regular gain scheduling can be seen in Figure 2-7. While this method leads to a significant increase in performance at higher wind speeds, the most critical problem of the RHPZ is not addressed around the rated wind speed.

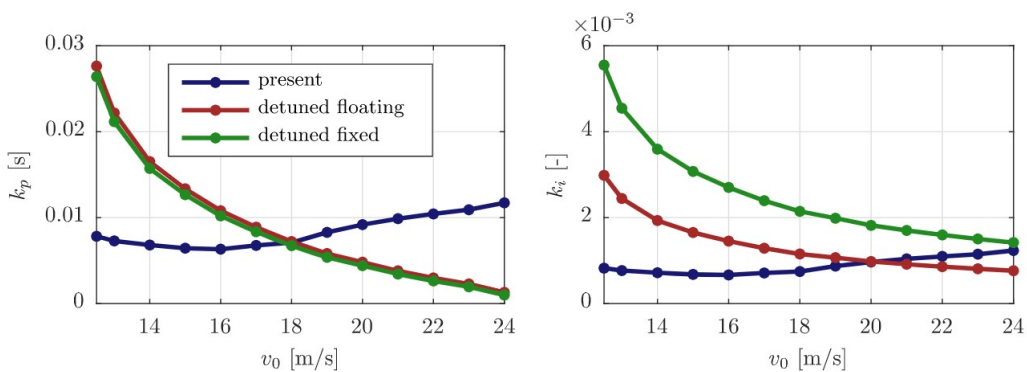


Figure 2-7: Robust gain scheduling compared with gain scheduling for a regular wind turbine and detuned gains of a floating wind turbine. [8]

In [24], the author takes an interesting approach to the control problem. The paper recognizes the induced wind speed from tower top motions as the destabilizing factor. This wind speed

is estimated by measuring platform pitch motions, and corrected for with a type of pseudo-feedforward gain:

$$g_{wv}(V_w) = \frac{d\theta_b}{dF_a} \frac{dF_a}{dV_w} \quad (2-6)$$

V_w is the estimated apparent wind speed, θ_b is the blade pitch and F_a is the thrust force. However, rotor thrust and rotor torque are not equally influenced by this induced wind speed. Therefore, during constant torque operation (above rated), a different rule is used to not interfere with the blade pitch feedback controller.

$$g_{wv}(V_w) = \frac{d\theta_b}{dT_a} \frac{dT_a}{dV_w} \quad (2-7)$$

Results are presented in the time domain and look promising. An interesting addition would be to see how the feedforward gain modifies the plant for SISO control, and what happens with the RHPZ.

MIMO control In a MIMO controller for wind turbines for above rated operation, additional inputs are used besides the rotor speed, and additional outputs are used besides the blade pitch. For example, tower motions can be measured and used for feedback, and the generator torque can be used as an additional control input. As [9] notes, controllers that use multiple inputs and outputs in separate SISO loops are common. While this method does not take into account interaction between the different variables, the author shows that it can be effective in FWTs. Parallel path modification is used to compensate non-minimum phase zeroes. As shown in Figure 2-8, the nacelle motion is fed back in order to control the generator torque. This loop is used to modify the plant's characteristics, removing the right half-plane (RHP) zero. While a higher bandwidth can be reached using this strategy, it increases torsion fatigue on turbine's shaft.

This method was first used in a fixed bottom wind turbine in [37]. In fixed bottom wind turbines, RHP zeroes occur at natural frequency of the tower's first bending mode. Because the zeroes occur at much higher frequencies, this is in general less problematic.

As [15] mentions, MIMO control is not a perfect solution to the control problems of FWTs. Performance is still bounded by the design of the generator. If the generator is not designed to accommodate for large fluctuations of the electrical current, control actions are limited. If these bounds are too tight, torque control might not be able to remove the RHPZ.

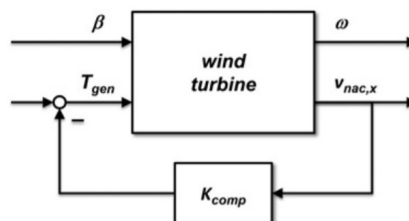


Figure 2-8: Parallel path modification. The feedback loop is applied to modify the wind turbine system. [9]

Another MIMO strategy is the model predictive controller (MPC) discussed in [26]. In MPC, optimal control actions are continuously selected based on measured variables and a model of the system. While the study shows promising results, model based control is not popular in the industry as it relies on a simplified model of the wind turbine. Therefore, unmodeled dynamics can influence its robustness. However, as [27] notes, MPC is especially suited to operate with disturbance information. Wind turbines can be equipped with Light Detection and Ranging (LIDAR) systems [28] to measure the incoming wind. This information can be used in the MPC.

2-3-2

Modelling For a more theoretical approach to this problem, a model is required. Specifically, a linear model is useful, as most analysis and design tools for control systems are based on linear systems. As a wind turbine is a highly non-linear system, a linearized model is necessary. A linearization is only accurate close to a certain steady state operation point, defined by a wind speed. However, while it does not accurately model the system outside that region, it still indicates the characteristics of the system.

When looking at a linearized model, the problem of negative aerodynamic damping translates to a RHP zero pair. One important characteristic of a RHP zero is that it leads to initial undershoot, seen in Figure 2-9 [38]. This initial overshoot in response to a step input is also seen in the transfer function from wind speed to rotor speed: if the wind speed increases, the wind turbine will initially pitch back. Then, due to the controller pitching the blades, the wind turbine will pitch forward and settle.

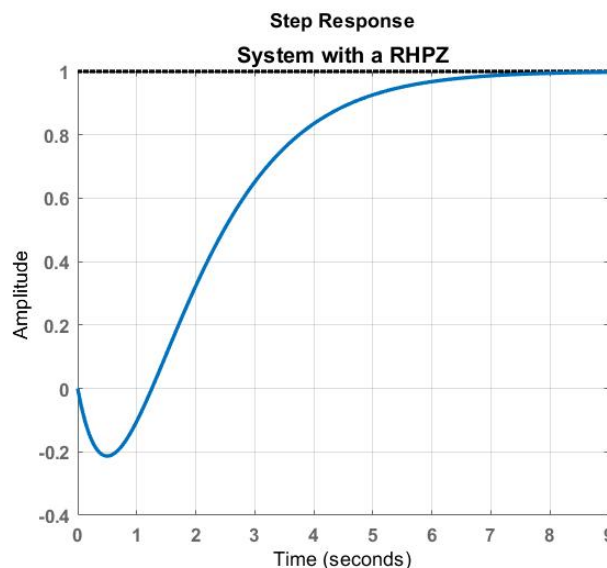


Figure 2-9: Initial undershoot caused by a RHP zero. The system is defined as: $G(s) = \frac{-s+1}{s^2+2s+1}$

Closed loop feedback control is limited for systems with RHP zeroes. Increasing the gains will shift the poles of the closed loop system towards the zeros. Poles in the RHP will cause instability, so the controller gains should be small. This is the controller for a regular wind

turbine is infeasible for the same wind turbine on a floating platform, and the gains should be detuned.

In a bode plot, a RHP zero shows the magnitude behavior of a regular zero, but with a 90 degree phase drop instead of an increase. This essentially sets a limit to the bandwidth, as the phase margin will be too small after the frequency of these zeroes, making the system unstable. The bandwidth is defined as the crossover frequency: the frequency where the open loop system gain is 0 dB. This determines how fast the controller is. The phase margin is determined by the phase at this crossover frequency, specifically the distance from -180 degrees. A system is unstable when for a certain frequency, the gain is over 0 dB and the phase is under -180 degrees. Therefore, the gain margin is used to determine robustness, or whether the system is close to an unstable response. The frequency domain behavior of the RHP zero is shown in Figure 2-10. This example is based on the following transfer functions:

$$RHPZ = \frac{s - 0.1}{s(s + 1)} \quad LHPZ = \frac{s + 0.1}{s(s + 1)} \quad (2-8)$$

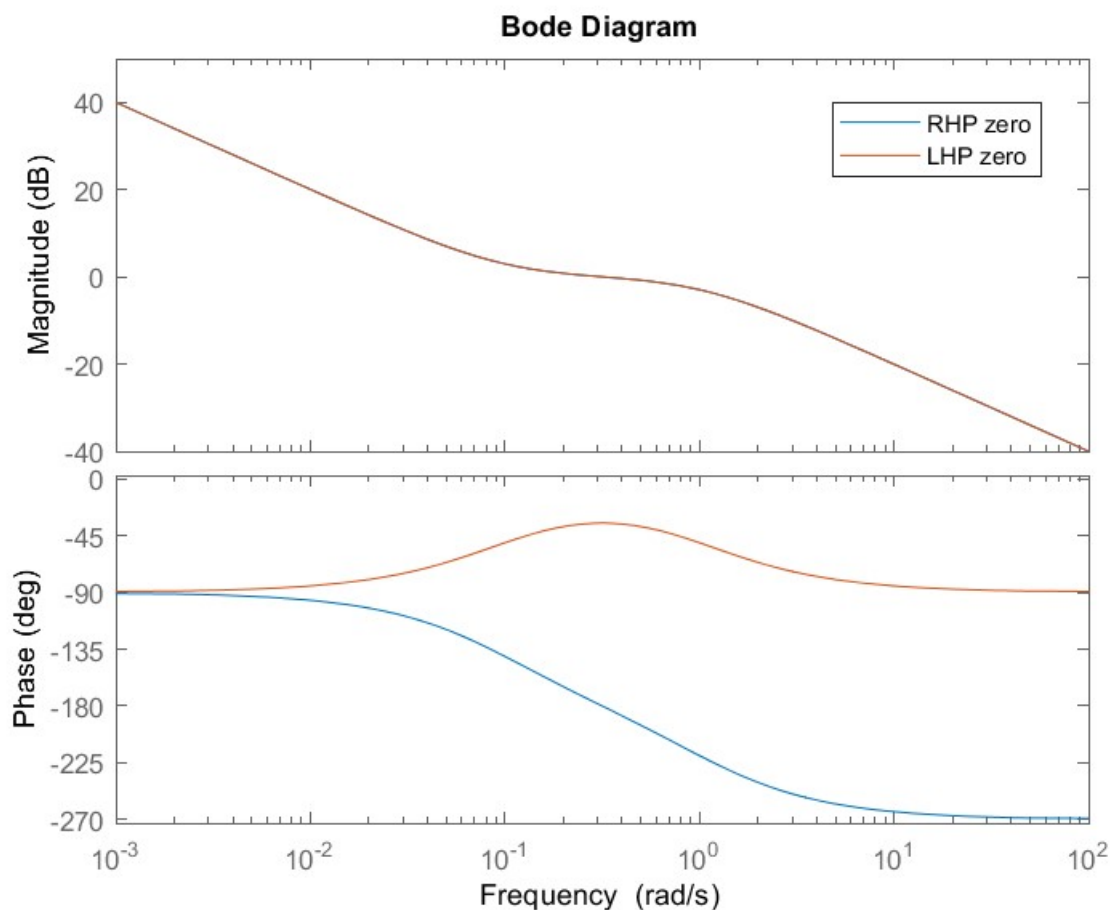


Figure 2-10: Bode plot comparing systems containing a RHP zero and a LHP zero. The gain behavior is exactly the same, but the RHP zero's phase decreases.

In a FWT, the pair of RHP zeros causes the phase to drop below -180 degrees around the resonance frequency of the rigid body pitch mode. This means that the bandwidth must be lower than this frequency to achieve a sufficient phase margin.

2-4 DTU 10MW Reference Turbine with SWE Triple Spar platform

For this thesis, a specific floating wind turbine had to be selected for which the controller had to be designed. A practical choice is a wind turbine for which the design parameters are freely available. Technical University of Denmark (DTU) has defined a 10 MW reference turbine [39], for which Stuttgart Wind Energy (SWE) has designed a triple-spar (semi submersible) floating platform [40]. Conveniently, a FAST (Fatigue, Aerodynamics, Structures, and Turbulence) v8 model exists for this floating wind turbine, provided by the authors of [41], which enables simulation in Simulink by Matlab. Furthermore, linearizations for this FWT were acquired via simplified low order wind turbine (SLOW) [15].

This choice was also motivated by the current trend in offshore wind turbines towards larger rotor size and rated power, and the fact that larger structures generally have lower natural frequencies, exacerbating the problems mentioned.

2-5 Reset Control

In this section, an introduction to reset control is given. Reset control is a non-linear control technology that aims to overcome limitations of linear control. As it relies on a base linear system augmented with a reset element, the working principles behind reset control are easily understood. The general form is shown in figure 2-11: a regular feedback loop, where the shifted rectangle is used to show that it is a reset controller. However, as many methods of system analysis are based on LTI systems, analysis of systems containing reset technology is not as straightforward.

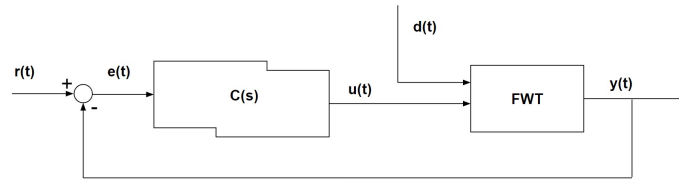


Figure 2-11: Diagram of closed loop reset control for a FWT. The shifted rectangle represents a reset controller. The signals: $r(t)$ is the reference, in this case the rated rotor speed. $e(t)$ is error signal. $u(t)$ is the blade pitch angle. $d(t)$ is the disturbance, in this case the wind speed. $y(t)$, the output, is the measured rotor speed.

This chapter will briefly discuss the history of the technology, and then move on to the characteristics. A few controllers with reset technology will be visited, each having different advantages and disadvantages.

Notation As research into reset control has not been very consistent in its notation, for this thesis some standards are used, mostly based on [10]. Firstly, the different states: x_p is the plant state, x_r the controller internal state, and $x = [x_p \ x_r]^T$. These subscripts also apply to the state-space representation of the (base linear system of the) plant, the reset controller and the closed-loop system (e.g. A_p , A_r and A). The reset time t^+ is used to define the value of a signal after reset (as opposed to t^- which is the same time but before the reset occurred). e.g. $x_r(t^+)$ is the controller state after reset. The error $e = r - y$, with reference r and output y (see also Figure 2-11). The discrete system matrices are denoted with subscript R , for instance: A_R is the system matrix that defines the resets. The plant's dimension is known as n_p , the controller's dimension is n_r which can be split up in n_{ρ} , the number of reset states and $n_{\bar{\rho}}$, the number of controller states that do not reset.

2-5-1 Origins

Reset control is a control technology that was developed by J.C. Clegg in the 1950s [23]. The Clegg integrator (CI) is the simplest reset controller, which resets the controller state to zero when the error signal crosses zero. Its describing function (the describing function is essentially a way to make a bode plot for a non-linear system, this will be explained later). still has the same -20 dB magnitude slope, but only has a phase loss of 38 degrees, which gives a phase advantage of 52 degrees over a linear integrator. In the time domain, a reduction in

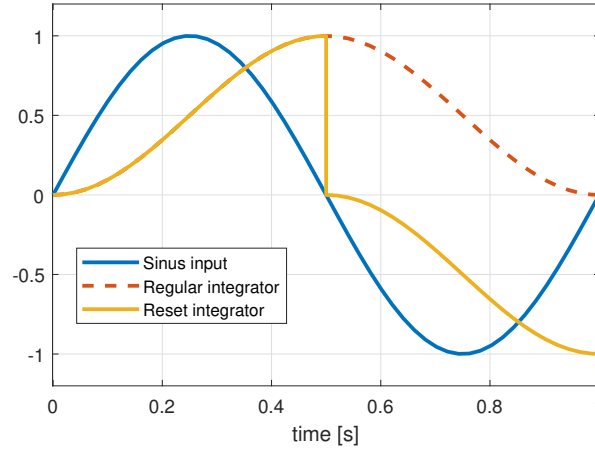


Figure 2-12: Output of the Clegg Integrator with sinusoidal input, compared to a regular integrator.

overshoot can be achieved. This can intuitively be understood: the integrator control signal starts by pushing the error towards zero more and more over time. When the error crosses zero, the output of an integrator is still positive, pushing in the same direction, away from a zero error again. This introduces overshoot. By setting the integrator state to zero at that instant, the control signal won't push in the wrong direction. This effect can be seen in figure 2-12, where it is obvious that due to the resets, the control signal will never have the opposite sign to the error. Therefore, the reset condition is sometimes chosen to be $e(t)u(t) \leq 0$, resulting in the same behavior.

The CI is defined as follows:

$$\begin{aligned} \dot{u}(t) &= e(t) & \text{when } e(t) \neq 0 \\ u(t^+) &= 0 & \text{when } e(t) = 0 \end{aligned} \quad (2-9)$$

In the 70s, another controller that uses reset technology has been introduced by Horowitz et al: first-order reset element (FORE) [42]. The FORE is basically a first order low-pass filter that resets its state at the zero crossings of the error. Figure 2-13 shows how it works. This design achieves the same phase lag improvement as the CI but the FORE is described as follows:

$$\begin{aligned} \dot{u}(t) &= -au(t) + Ke(t) & \text{when } e(t) \neq 0 \\ u(t^+) &= 0 & \text{when } e(t) = 0 \end{aligned} \quad (2-10)$$

A more general description for a reset controller (taken from [10]) also enables the use of zero crossings of another function than the error function to define reset times, and the possibility to use a function to describe the reset value (instead of zero):

$$\begin{aligned} \dot{u}(t) &= e(t) & \text{when } c(t) \neq 0 \\ u(t^+) &= a(t) & \text{when } c(t) = 0 \\ u(0) &= u_0 \end{aligned} \quad (2-11)$$

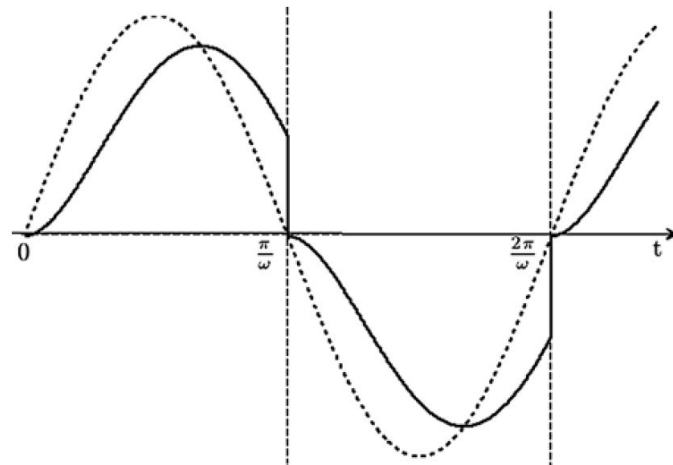


Figure 2-13: Output of the FORE (solid) with sinusoidal input (dashed) [10]

2-5-2 Characteristics of reset control

Often, a reset controller is regarded as a base linear system (which can be represented by a transfer function), in combination with a reset element (a CI). Stability of the base linear system doesn't guarantee stability of the full reset control system and isn't necessary either for stability of the full system [43]. The implications of this are significant. Firstly, a more intricate analysis of stability of a reset control system is necessary, since it can't be assumed by designing a stable base linear system. Secondly, design of a reset system doesn't necessarily start with a stable base linear system. This implies a more complicated design process.

It has been shown through simulations and experiments (for example in [44]), that reset control can be used to achieve performance that is out of the reach of linear controllers in both time and frequency domain, mainly reducing overshoot while retaining other design objectives. In the frequency domain there is a 52 degree improvement in phase loss as compared to a linear integrator, based on describing function analysis, beating the Bode gain-phase relationship.

Reset control also has some downsides. Firstly, there is an added complexity in design and analysis of these controllers when compared to linear alternatives. There are more parameters to be tuned, only after a choice out of the variety of reset controller designs has been made.

Sensor noise can be a problem for reset controllers. The noise can trigger many resets in a short time if the system is at rest. Therefore, in practice a reset band is often required, which will be discussed in the next section.

Reset controllers can also have problems regarding well-posedness of the solutions [45]. This can result in pathologies: deadlock, livelock and Zenoness. Livelock or beating occurs when the system reaches the reset condition multiple times in zero time. An example of this can occur with the alternative reset condition $e(t)u(t) \leq 0$ and a CI parallel to a linear integrator, because then $u(t)$ can reset to a positive value even if $e(t)$ is negative, leading to continued resets without any results.

Deadlock occurs when no continuation of the solution exists. This can happen when the flow set and the jump set aren't well defined and a jump can lead to a solution in neither set.

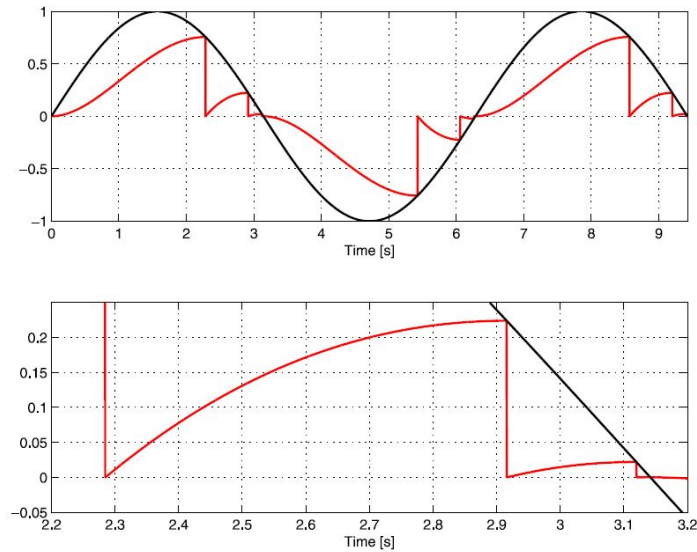


Figure 2-14: A CI in a feedback loop leading to Zeno solutions. After each reset the time until the next reset decreases. [10]

The concepts of flow set and jump set are derived from hybrid systems theory. The flow set is the portion of all possible states for which the system evolves following the continuous equation and the jump set is the set of states for which the system jumps (in this case: a reset). Zenoness, its name derived from Zeno's paradox of an athlete overtaking a tortoise, means that infinite solutions occur in finite time. This happens when after each reset the time until the next reset decreases. This effect is illustrated in figure 2-14.

Finally, a reset integrator can have trouble reaching a steady state. Often, limit cycles are observed [46], where the system will keep repeating the same flow and jump behavior. Several ways of solving this problem have been proposed over the years, each introducing new difficulties, which will also be discussed.

Note that not all of these downsides are very important when reset control is applied in a system with a lot of disturbances. Limit cycles are observed when the system tries to settle under constant disturbance, but for floating wind turbines, the disturbance (wind and waves) is highly varying.

2-5-3 State-Of-The-Art in Reset Control

In this section, more advanced reset control system designs will be shown. These controllers try to overcome the difficulties discussed in the previous section.

SORE The Second-Order Reset Element or SORE is a logical expansion on the FORE, proposed in [47]. It is a reset element based on a second order low-pass filter. The linear variant is defined by the transfer function $C_{lp} = \frac{\omega_p^2}{s^2 + 2\beta_p\omega_p s + \omega_p^2}$. The SORE based on this

controller is defined as

$$\begin{aligned} \dot{x}_r(t) &= A_r x_r(t) + B_r e(t) && \text{when } e(t) \neq 0 \\ \dot{x}_r(t^+) &= A_\rho x_r(t) && \text{when } e(t) = 0 \\ u(t) &= C_r x_r(t), \end{aligned} \quad (2-12)$$

where the state space matrices are

$$A_r = \begin{bmatrix} 0 & 1 \\ -\omega_p^2 & -2\beta_p\omega_p \end{bmatrix} \quad B_r = \begin{bmatrix} 0 \\ \omega_p^2 \end{bmatrix} \quad C = [1 \quad 0]. \quad (2-13)$$

In the paper, the case where all the controller states are reset is considered, i.e. $A_\rho = \begin{bmatrix} 0 & 0 \\ 0 & 0 \end{bmatrix}$. Other reset matrices can be considered for future designs. The paper shows that a SORE is a viable candidate for improving on regular second order filters, improving bandwidth while still satisfying other specifications. It is a good example of the working of a reset controller with two integrators, which can also be used in PI²D design. While the mathematical frameworks that are used in most papers on reset control do take into account the possibility of higher order reset controllers, implementation of such a design is new.

PI+CI In [11], a parallel structure is proposed that combines a normal PI controller with the Clegg Integrator (see figure 2-15). A reset percentage p_{reset} , given by $\frac{T_i}{T_{ir}}$ can be defined that determines what part of the integrator state is reset. The advantage of this controller is that it still achieves an improvement on phase loss (proportional to the reset percentage), while also benefiting from the removal of steady-state errors like a regular integrator. Depending on how you look at it, this can be a big sacrifice (because phase loss is added), or a good trade-off that compensates some of the disadvantages of a pure CI.

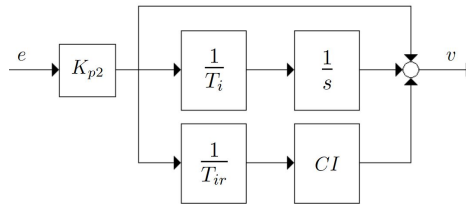


Figure 2-15: PI+CI controller structure. The parallel connection means that only part of the controller state is reset, defined by the reset percentage (the ratio of the linear and CI integrator gains) [11]

Reset Band When the error signal is very noisy, the error could cross zero very often in little time. To avoid this, a reset band δ can be defined, introduced in [12], such that the controller only resets when the band is entered (while the error is moving towards zero). If it is chosen adequately, the noise will stay within the reset band and not trigger any resets. In figure 2-16, a time domain simulation of a FORE with reset band is given. It is shown that the describing function of a reset controller with reset band can actually have a bigger phase advantage than a normal reset controller. This is illustrated in Figure 2-17. The figure shows that for a reset band the size of the amplitude of the input signal, the phase is 90 degrees

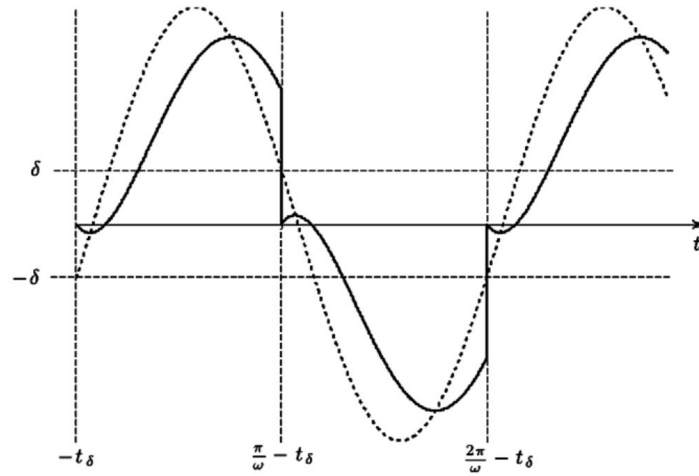


Figure 2-16: Response to a sinusoidal input of a FORE with reset band. The dotted line is the error, the solid line is the controller's output. [12]

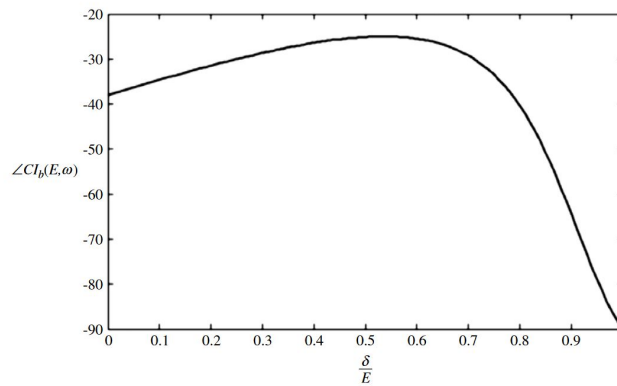


Figure 2-17: Phase of the FORE with reset band, depending on the relative size of the reset band $\frac{\delta}{E}$. [12]

(which is expected because no inputs will occur). An optimum is found somewhere between a reset band of zero (no reset band) and one that is bigger than the input signal. The reset band can also be variable. By defining a reset surface that relies on both the error e and its derivative \dot{e} , a more advanced reset band can be defined. For low frequencies (and therefore small values of \dot{e}) it behaves more like a normal reset controller, and for high frequencies it behaves more like a linear integrator, because then the reset band is wider, preventing resets.

FORE with setpoint stabilization Another way to tackle the problem of limit cycles is presented in [48]. Here, a feedforward gain is used that defines the after-reset controller state ($x_r^+ = -Fr$). The gain F is defined by the static gain of the system:

$$F = \frac{1}{C_p A_p^{-1} B_{pu} k}, \quad (2-14)$$

where k is the FORE's gain, A_p and C_p are the plant's state-space matrices and B_{pu} is the input matrix for control signals (i.e. without disturbances). For this definition, it is important that A_p is invertible. The authors do note however that this system is still affected by disturbances. Also uncertainties in the static gain will lead to worse outcomes. The same feedforward gain can be added to different reset controllers.

Reset Control with resets at fixed time instants Using predetermined reset times can make a reset control system easier to analyze, as no uncertainty exists about when a reset will occur. This is important for results on stability. In [49], such a system is designed. The resets occur at a frequency that is to be determined in the design process. However, unlike in the most basic reset controllers, the after-reset value of the controller state x_r is not zero. The after reset value of the controller is defined by: $x_r(t^+) = \rho_k(x, r)$ such that it depends on the current state of both the plant and the controller as well as the reference:

$$\begin{aligned} \dot{x} &= Ax + Br && \text{when } t \neq t_k \\ x_r(t_k^+) &= \rho_k(x, r) && \text{when } t = t_k \\ y &= Cx, \end{aligned} \quad (2-15)$$

with $\Delta t_k = t_k - t_{k-1}$.

Then, ρ is optimized using a quadratic performance index. Now another advantage of predetermined reset times arises, as it is shown that when the reset times are spaced equally, the optimized function $\rho(x, r)$ is constant and therefore LTI. This effectively turns the system into

$$\begin{aligned} \dot{x} &= Ax + Br && \text{when } t \neq t_k \\ x_r(t_k^+) &= Gx + Fr && \text{when } t = t_k \\ y &= Cx. \end{aligned} \quad (2-16)$$

However, it is also shown that the optimal solution for $\rho(x, r)$ does not always lead to a robustly stable system. Therefore, a parameter μ is defined that slides between the optimized system and the base linear system ($\mu = 0$ gives the base linear system, $\mu = 1$ gives the solution to the optimization). Note that this controller uses a similar philosophy as the controller with setpoint stabilization, as it effectively uses a feedforward gain to adjust the after reset value. However, the resets in this controller can also take place when the error is not zero, and therefore the error can be used to determine the after reset value, possibly leading to better results. However, this makes the use of a state estimator necessary in many practical applications.

While this design shows very good results, the design process is complicated and relies on knowledge of the full state of the system. It makes sense that it would yield good results because it behaves almost like a model predictive controller, because every reset instant, an optimal control action is selected. Then, it briefly evolves according to the linear system, before it is reset to an optimal value again. It makes the controller require some computational power and an accurate model of the closed loop base linear system is required to define $\rho_k(x, r)$.

Temporal Regularization Because well-posedness can be a problem for reset controllers (discussed in section 2-5-2), it is important to add time-regularization to the system. Often, this is done by adding a condition to the reset action, for example when applied to the Clegg Integrator:

$$\begin{aligned} \dot{u}(t) &= e(t) \quad \dot{\tau} = 1 && \text{when } e(t) \neq 0 \text{ or } \tau < \rho \\ u(t^+) &= 0 \quad \tau^+ = 0 && \text{when } e(t) = 0 \text{ and } \tau > \rho \end{aligned} \quad (2-17)$$

This means a reset can only occur when ρ time has passed after the last reset. τ is an auxiliary variable that keeps track of how much time has passed since the last reset. It has been shown that temporal regularization is also important for results on stability [50]. It guarantees that the reset system's state will evolve following the continuous system equation for a minimum amount of time, which is required for some stability conditions. In further analysis, it is assumed time regularization is used where necessary.

Generalized reset controller In [51], a general form for reset controllers is defined including some of the aforementioned technologies: PI+CI parallel structure, fractional order integrators, reset at fixed time instants, and it includes the possibility to introduce a feedforward gain. The feedforward gain is used to avoid limit cycles. The general formulation of the reset controller is:

$$\begin{aligned} D^\alpha x_r(t) &= A_r x_r(t) + B_r e(t) && \text{when } e(t) \neq 0 \\ x_r(t^+) &= A_{Rr} x_r(t) + \frac{K}{n_{\mathfrak{R}}} B_{Rr} r && \text{when } e(t) = 0 \\ u_r(t) &= C_r x_r(t) + D_r e(t) \end{aligned} \quad (2-18)$$

A few things need to be cleared up in this description of the controller. Firstly, the reference is assumed to be constant. $n_{\mathfrak{R}}$ is the number of states that are reset (defined by $A_{Rr} = \begin{bmatrix} I_{n_{\mathfrak{R}}} & 0 \\ 0 & 0_{n_{\mathfrak{R}}} \end{bmatrix}$). Matrix $C_r = c_r \begin{bmatrix} 0 & 1 \end{bmatrix}$. This makes c_r the integrator gain and $\alpha \in \mathbb{R}^+$ the fractional order of the integrator.

In the same paper [51], a general version is given for the reset controller with resets at fixed time instants. This controller looks very much like the one given in 2-18, but resets at $t = t_k$ and includes the error signal in the jump equation (as the error is not necessarily zero at the reset instants).

As has been discussed in the paragraph on the setpoint stabilizing controller, which also uses a feedforward gain, limit cycles can still be induced by parameter uncertainties and disturbances. In [52] an adaptive algorithm is used to adapt the feedforward gain to achieve perfect reference tracking. However, this yields a much more complicated controller that also takes longer to converge. It could be suitable for an application that has some time varying parameters, that are constant for a certain amount of time. Then, the adaptive algorithm can adjust to occasional changes in the system to avoid limit cycles, while still having superior behavior to a linear controller. If these disturbances and parameters change continuously, this method might just be inferior to a simple linear controller.

HIGS In 2017, a hybrid integrator gain system (HIGS) controller has been developed, with similar advantages as reset control systems [13]. It tries to avoid resets like in a CI, as it might discard the whole integrator state prematurely and it introduces higher frequency harmonics

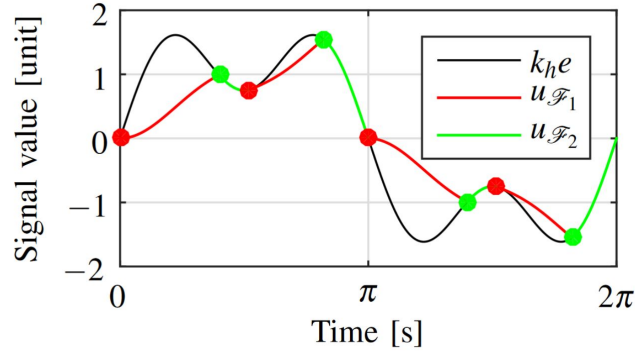


Figure 2-18: Time domain response of the HIGS. For the red segments, the response is like that of an integrator. For the green segments, it is a proportional gain. Note that when switching modes, the state is saved [13].

in the signal. However, the philosophy behind the design is similar: the input and output of the hybrid integrator gain controller always have the same sign, such that the controller always pushes towards a zero error, which is not the case for a linear integrator. This is most clearly seen in figure 2-18. The HIGS can be described as:

$$\begin{aligned} \dot{x}_h(t) &= \omega_h e(t) && \text{when } (e, u, \dot{e}) \in \mathcal{F}_1 \\ 0 &= -x_h(t) + k_h e && \text{when } (e, u, \dot{e}) \in \mathcal{F}_2 \\ u &= x_h \end{aligned} \quad (2-19)$$

The flow sets \mathcal{F}_1 & \mathcal{F}_2 are defined as:

$$\begin{aligned} \mathcal{F}_1 &:= \{(e, u, \dot{e}) \in \mathbb{R}^3 \mid eu \geq \frac{1}{k_h} u^2 \wedge (e, u, \dot{e}) \notin \mathcal{F}_2\} \\ \mathcal{F}_2 &:= \{(e, u, \dot{e}) \in \mathbb{R}^3 \mid u = k_h e \wedge \omega_h e^2 > k_h \dot{e} e\} \end{aligned} \quad (2-20)$$

Note from Equation 2-19 or Figure 2-18 that if the proportional gain is infinite, the HIGS turns into a CI. A short describing function analysis has been performed for different values of k_h and ω_h in [14], which is shown in figure 2-19. It shows the same phase advantage as a normal reset element, with low-pass behavior. Intuitively, this is expected. For low frequencies, the integral state will become very large, and the controller will function according to \mathcal{F}_2 , as a proportional gain. For high frequencies, the derivative of $k_h e$ will be high, so it will function more like a CI.

CgLp A very recently developed reset controller is the constant gain, lead in phase (CgLp) element [1]. It uses the phase advantage of a reset element to create a filter that simply adds positive phase to a system. Now of course, this seems like a fantastical idea which could solve almost any linear control problem, but keep in mind that disadvantages of reset control still apply to this filter: while the describing function gives a good approximation of what this filter achieves, it is not fully accurate. The filter consists of a linear lead filter in series with a low pass filter with a reset element (either a FORE or a SORE). Figure 2-20 shows how the gain behavior of these elements essentially cancels out. However, as the phase loss of the

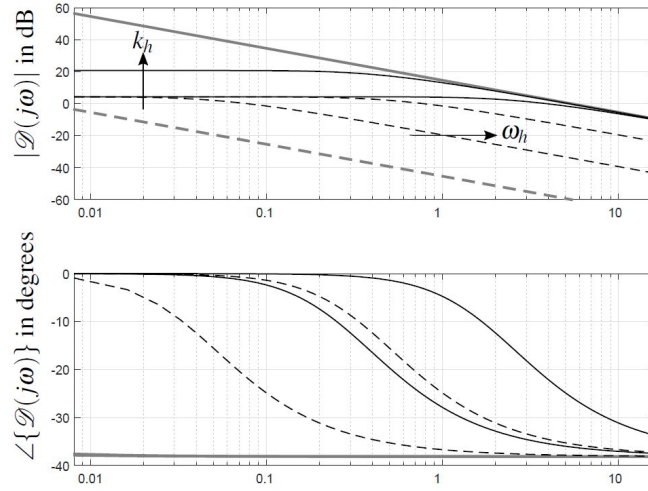


Figure 2-19: Describing function of the HIGS for changing parameters [14]

reset integrator is much lower than the phase gain of a linear lead element, a net positive phase can be seen.

The philosophy is that normally, an integrator should not be active around the bandwidth of the system. Therefore, the phase advantage of a regular reset integrator would not add phase in the desired frequency domain. Normally, a differentiator is used to add phase around the bandwidth. This has the downside that it adds gain at high frequencies. The desire for a filter that adds phase around the bandwidth like a differentiator without affecting gain performance, inspired this controller.

The CgLp with a second order reset element is defined as a state space system [1]:

$$\begin{aligned}
 A_r &= \begin{bmatrix} 0 & 1 & 0 & 0 \\ -\omega_{r\alpha}^2 & -2\beta_r\omega_{r\alpha} & 0 & 0 \\ 0 & 0 & 0 & 0 \\ 1 & 0 & -\omega_f^2 & -2\omega_f \end{bmatrix} & B_r &= \begin{bmatrix} 0 \\ \omega_{r\alpha}^2 \\ 0 \\ 0 \end{bmatrix} \\
 C_r &= \begin{bmatrix} \frac{\omega_f^2}{\omega_r^2} & 0 & \left(\omega_f^2 - \frac{\omega_f^4}{\omega_r^2}\right) & \left(\frac{2\beta_r\omega_f^2}{\omega_r} - \frac{2\omega_f^3}{\omega_r^2}\right) \end{bmatrix} & D_r &= [0] \\
 A_\rho &= \begin{bmatrix} \gamma I & 0 \\ 0 & I \end{bmatrix}
 \end{aligned} \tag{2-21}$$

A_ρ is the reset matrix, which sets the states on a reset. In a classic reset element, $\gamma = 0$, but it can be selected anywhere in $[-1, 1]$, with $\gamma = 1$ being the base linear system. ω_r is the corner frequency for the reset element and the lead filter. ω_f is the frequency of the pole in the lead filter. $\omega_{r\alpha}$ is the adjusted corner frequency, because due to non-linearity, the corner frequency shifts with a factor α .

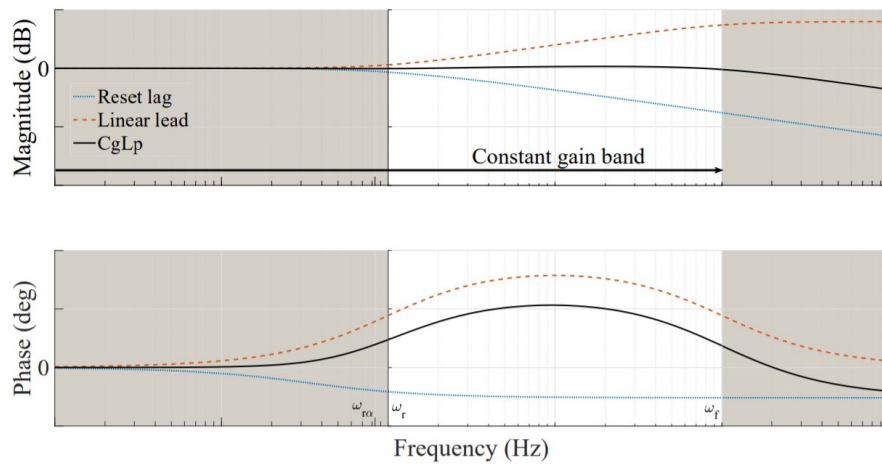


Figure 2-20: Describing function of the CgLp [1]

Controller Design

In this chapter, the design of the non-linear reset based controller will be discussed. Firstly, a linearized version of the DTU 10MW FWT with the SWE triple spar platform will be introduced, which is used for the controller design. A linear model is useful in order to take advantage of the many design tools available for linear systems. Then, a linear baseline controller will be defined to compare any results with. Then, the reset controller is designed using loop shaping, based on describing function analysis for the non-linear parts in the controller. With the describing function, the behavior of the non-linear controller can be visualized and analyzed in a bode diagram.

To help focus on the research question at hand, a single control problem is addressed. As mentioned in Chapter 2, the right half-plane (RHP) zeroes for above rated operation are most problematic in the region close to the rated wind speed. Therefore, a linearization of the system around that wind speed is selected, and a controller is designed for that specific point.

3-1 Linear model

In [15], a simplified low order wind turbine (SLOW) model is introduced. It was developed for faster simulation and design optimization than existing software such as FAST, as well as for linear system analysis. Linearizations made in SLOW for the DTU 10MW with SWE triple spar platform were provided by the author of the model. A bode plot from blade pitch to rotor speed is shown in Figure 3-1.

In this model, the RHP zeroes that cause the phase to drop under -180 degrees are located at a frequency of 0.252 radian per second. Another pair of RHP zeroes is located at 2.56 radian per second, corresponding to the fore-aft bending mode of the tower. The last pair of zeroes at 0.034 radian per second (the downward peak) corresponds to the surge mode of the platform. This means that the blade pitch has relatively little effect on variations of the rotor speed at this frequency, as these variations are largely dictated by change in relative wind speed due to the surge motions.

As the plot shows, the slope of the phase near -180 degrees is gentle. This means that additional phase at this frequency will increase the frequency at which the phase crosses -180 degrees. Therefore, adding phase can have an impact on the bandwidth and/or stability margins. On the other hand, the slight peak in magnitude at this frequency limits the increase in proportional gain, as that will compromise the gain margin.

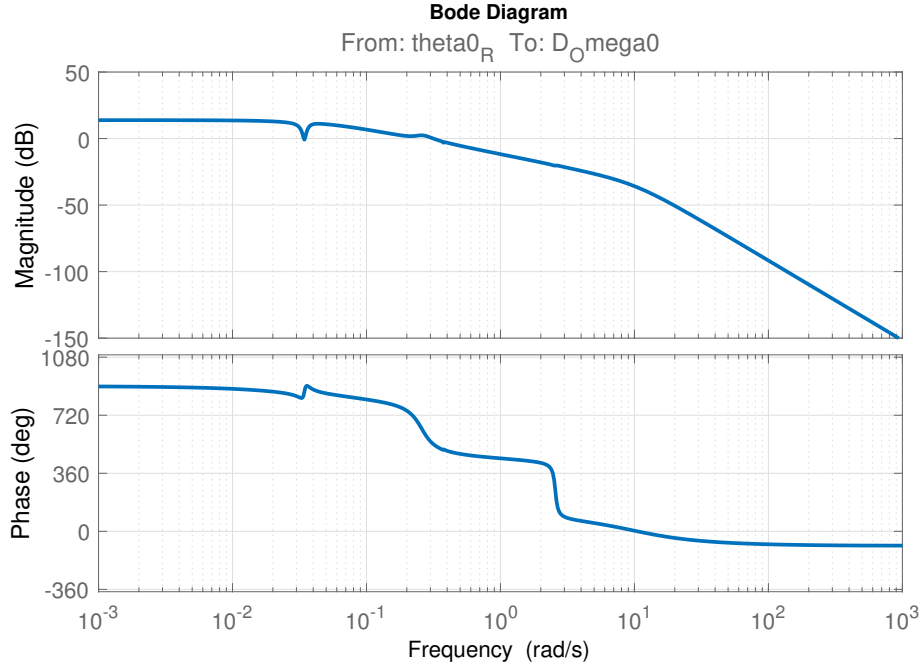


Figure 3-1: Bode plot from blade pitch to rotor speed of the linearized DTU 10MW with SWE triple spar platform at a wind speed of 12 m/s, derived using SLOW [15].

3-1-1 Linear baseline controller

A baseline controller for the DTU 10MW was defined by DTU [53]. However, this controller is designed for a fixed bottom wind turbine, and should be adjusted for use on a floating wind turbine (FWT). In [41], the baseline controller is detuned to allow its use on a FWT. Damping factors of the poles associated with rotor dynamics and the platform pitch dynamics were considered. A trade-off is observed: A faster controller improved the rotor dynamics while worsening the platform pitch dynamics, and vice versa. An optimal compromise between these dynamics was selected. The controller is defined as follows:

$$K_p = \Delta K_p K_p^{DTU} \quad (3-1)$$

$$K_i = K_p T_i^{\text{new}} \quad (3-2)$$

In this formula, $\Delta K_p = 0.45$, and K_p^{DTU} is the original proportional gain defined by DTU (this gain is also determined by gain scheduling). The new time constant of the integral action was selected to be $T_i^{\text{new}} = 12\text{s}$. The same gain scheduling approach as in [53] was used.

To use this controller in the linearized model at 12 m/s wind speed, the scheduled gains are calculated, giving $K_p = 0.2221$ and $K_i = 0.0185$.

Additionally, [41] uses a low-pass filter to filter out any oscillations of the drivetrain torsion at its natural frequency of 11.3 radians per second. It is a second order low pass filter (see Equation 3-3) with a corner frequency ω_ω at 1.26 radians per second (0.2 Hertz) and a damping factor η_ω of 0.7. It reaches an attenuation of -38 dB at the drivetrain torsion natural frequency. However, the source cited by [41], uses an attenuation of -26 dB [54]. Therefore, using a corner frequency of $\omega_\omega = 2.5$ radians per second would suffice.

$$\frac{\Omega_{G,f}}{\Omega_G} = \frac{\omega_\omega^2}{s^2 + 2\eta_\omega\omega_\omega + \omega_\omega^2} \quad (3-3)$$

This baseline controller avoids exciting any oscillations at the natural frequency of the platform pitch. As a controller with resets will definitely excite higher frequencies, a comparison will likely favor the linear design. Therefore, controller gains are increased to get a faster baseline system with reduced robustness, in order to show how a CgLP can increase behavior. The new controller (see Equation 3-4) has a bandwidth of 0.127 radians per second, a gain margin of 4 dB and a phase margin of 40.7 degrees:

$$K_p = 0.4442 \quad T_i = 10s \quad \omega_\omega = 2.5 \quad \eta = 0.7 \quad (3-4)$$

3-2 Controller selection

First of all, one of the controller architectures introduced in Chapter 2-5 should be selected. In order to choose the most appropriate controller layout, a comparison must be made. Therefore, advantages and disadvantages are listed for each technology. These properties are compared with the desired properties for the floating wind turbine control problem. Firstly, a list of different choices is given.

1. Is the controller CI based, HIGS based, CgLP based, or a reset controller with fixed instant resets (FI)? These are the most elementary non-linear elements in a reset controller.
2. Should an (adaptive) feedforward gain be used? Feedforward gains are used to compensate for the DC-gain of a closed-loop system in order to reach the steady state. An adaptive algorithm might be necessary in the presence of disturbances or uncertainties, as the feedforward gain is not very robust.
3. Should a parallel structure be applied? The PI+CI architecture introduces a spectrum between fully linear and fully non-linear controller designs, adding a degree of freedom (p_{reset}), and similar architectures are possible for the other base controllers.
4. Is a Reset Band necessary? This should generally be applied in systems with noisy signals. Note that this option is only useful for a Clegg integrator (CI), as it is meaningless in the case of a HIGS controller or a controller with fixed reset instants.

For the choice for a base controller, the objective is considered. The reason for considering reset control is to add phase around the system bandwidth. If a controller is picked that replaces the linear PI controller of the system, the advantage of reset control is limited. This

is shown in Figure 3-2. The phase loss of the PI, close to the -180 degree crossing point of the system is only around 21 degrees. While a phase advantage in the lower frequency range can still be advantageous for system dynamics, the goal to increase the system bandwidth is not affected much by such a reset controller. Therefore, a CgLp is the obvious choice, allowing the designer to choose where added phase is necessary.

Another part of the objective is to design a simple solution compared to more advanced methods based on MPC or MIMO control. The controller with fixed reset instants discussed in Chapter 2-5 is still quite complicated, as it depends on full state feedback, and results heavily depend on the accuracy of the linear model. In this case, the accuracy of the linearization is only high close to the linearization point.

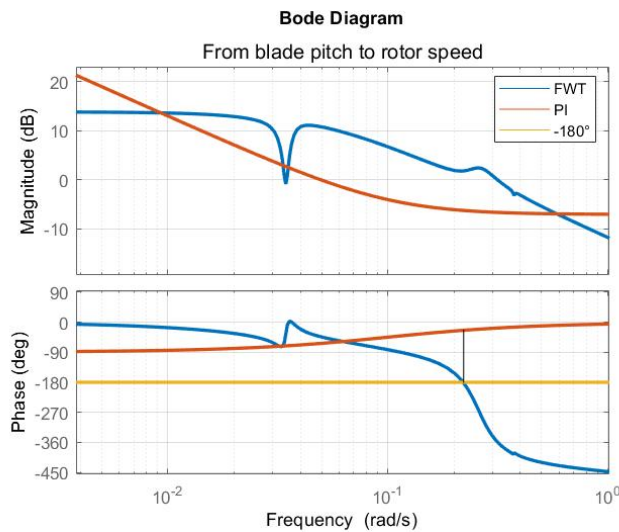


Figure 3-2: Bode plot of the linearized floating wind turbine at 12 m/s with the linear PI controller. It is shown in the figure that at the point where the system's phase crosses -180 degrees, the integrator of the PI is barely active anymore, leaving little room for improvement there.

After these considerations, the CgLp design seems most promising. Phase can be added at the desired frequency and its structure and design are based on the same intuitions as linear controller design.

A feedforward gain can be included to help reach a steady state, but the CgLp should have no problem reaching a steady state. Also, considering the amount of disturbances in a floating wind turbine, an adaptive feedforward gain would be necessary, increasing the controller's complexity. Therefore, a feedforward gain is not included in this design.

A parallel architecture can add an extra degree of freedom. However, the parameter λ (after reset value) already includes this degree of freedom with a much more simple implementation. Including a parallel gives the option to use different gains and filters for the non-linear and linear parts of the controller. However, this would add many parameters, making it much more complicated to find an optimal design. Therefore, just varying the after reset value λ gives sufficient degrees freedom for the CgLp and no parallel structure is included.

A reset band is generally used to deal with noisy signals, for example due to sensor noise.

As this thesis is based on computer simulations, the design will not include a reset band, but in practise it is important to have a method in place to prevent redundant resets. In conclusion, going forward in this thesis, the design of a CgLp type controller is described, without feedforward gain, reset band or parallel structure.

3-3 Tuning

The CgLp controller [1] is described by the state space representation in Equation 2-21. The parameters that must be determined are:

ω_r	First corner frequency of the lead filter
ω_f	Second corner frequency of the lead filter, corner frequency of the CgLp
$\omega_r\alpha = \alpha\omega_r$	Adjuster corner frequency for the SORE (determined by factor α)
β_r	Damping factor of the SORE and lead filter
λ	After reset value. Default value is $\lambda = 0$.

Tuning rules for the CgLp are mentioned in [1]. The rules for precision mechatronics were developed with loop shaping. A linear controller was first tuned according to the rules of [55]:

$$PID = K_p \left(\frac{s + \omega_i}{s} \right) \left(\frac{1 + \frac{s}{\omega_d}}{1 + \frac{s}{\omega_t}} \right) \left(\frac{1}{1 + \frac{s}{\omega_f}} \right) \quad (3-5)$$

Let us call the desired bandwidth ω_c , as in [1]. The corner frequency of integrator action is given by: $\omega_i = \omega_c/10$. A factor a is used to determine the frequency where the differentiator action starts: $\omega_d = \omega_c/a$. Differentiator action is tamed at $\omega_t = a\omega_c$ and a low pass filter to attenuate high frequency disturbances has corner frequency $\omega_f = 10\omega_c$. The factor a determines the amount of phase added by the differentiator action. However, a larger value of a also worsens tracking and precision performance (it lowers the loop gain at low frequencies and increases the loop gain at high frequencies). A typical value is $a = 3$. In [1], the CgLp adds phase to allow a decrease of value a , improving the tracking and precision performance. This is shown in Figure 3-3.

The parameters of the CgLp, listed in table 3-3, are defined as $\omega_r = \omega_c$, and $\omega_f = 10\omega_c$, the second corner frequency of the lead filter. While these values do not lead to an optimal phase lead at the desired frequency (since ω_r is set at the desired bandwidth and only defines the beginning of the phase lead region), these values are also optimized for time domain behavior.

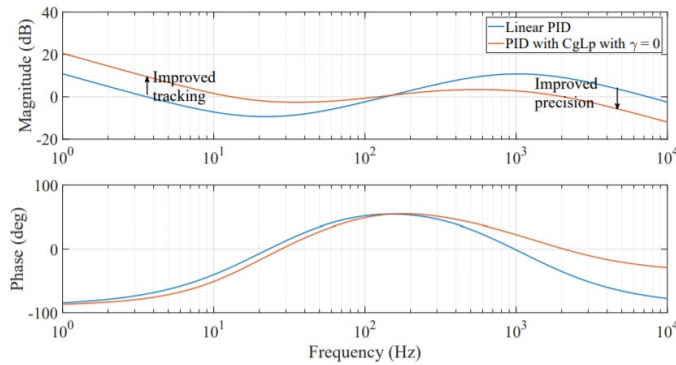


Figure 3-3: Bode plot with a comparison between a linear PID (as in Equation 3-5) and a PID with a CgLp, based on its describing function.

However, these rules were developed for precision mechatronics using a PID. The system characteristics for the FWT are very different and the baseline controller does not use derivative action. Therefore, following these rules is not appropriate, but a similar approach can be taken.

In this new approach for a FWT, the frequencies are determined first. As the baseline controller uses a low pass filter at 2.5 radians per second, ω_f is set to that value too, to achieve good attenuation at the drivetrain torsional natural frequency. As the baseline controller achieves a bandwidth of 0.127 radians per second, this is selected as the desired bandwidth for the non-linear controller. The tuning rule of $\omega_r = \omega_c$ is still used. Using a lower frequency can increase the phase more, but leads to badly timed resets.

As for after reset value λ , the results in [1] show that while a lower value leads to more advantage in the frequency domain, a value of 0.4 led to the best time domain behavior. For that value of λ , the correction factor α should be 0.9, meaning that $\omega_{r\alpha} = \frac{\omega_r}{0.9}$. The damping factor β_r is selected as 1. This leads to the a describing function shown in Figure 3-4, showing a phase advantage of 32.2 degrees at its peak and 25 degrees at ω_c .

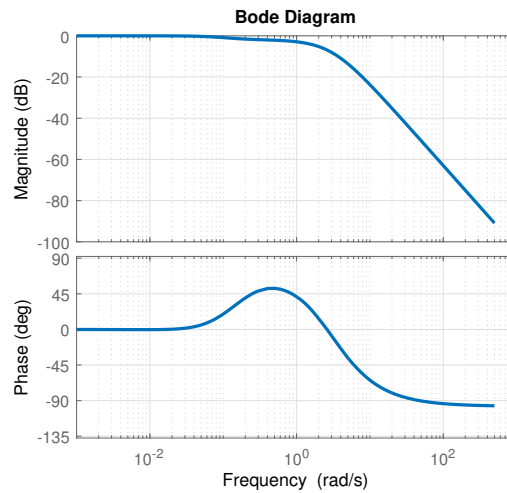


Figure 3-4: Bode plot of the describing function of the CgLp. Phase peaks at 32.2 degrees at 0.25 radians per second. At the desired bandwidth of 0.127 radians per second, the phase is 25 degrees.

Now, the PI controller should be designed. As shown in Figure 3-1, the slope of the gain plot is zero after the crossover frequency. Therefore, simply increasing the proportional gain K_p will, even with added phase, lead to a smaller gain margin. However, the increased phase of the open loop allows for stronger integral action. Using loop shaping, a controller was designed that achieves the same bandwidth as the linear baseline, but with an increased gain margin.

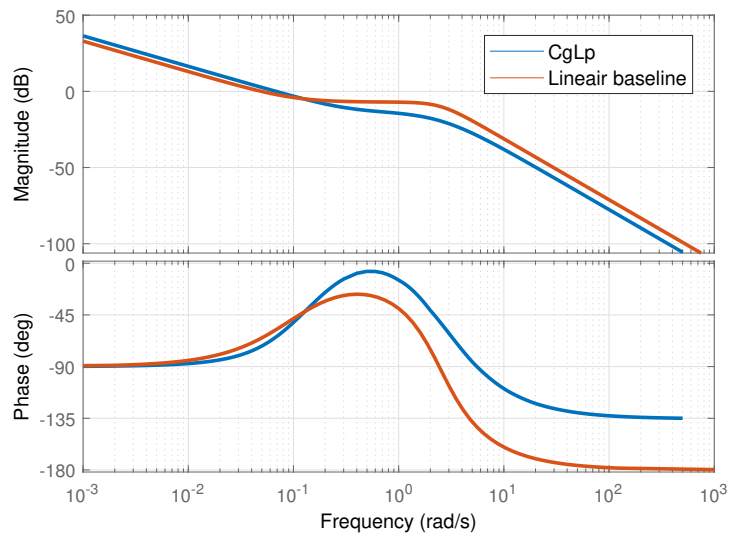


Figure 3-5: Bode plot of the describing function of the controller with CgLp (blue) and the linear baseline controller including the low pass filter (orange). The magnitude and phase lines cross over at the open loop crossover frequency, leading to the same bandwidth and phase margin. However, improved tracking performance and attenuation are shown, as well as a higher gain margin.

The bode plot of the open loop with the new controller with CgLp is shown in Figure 3-7.

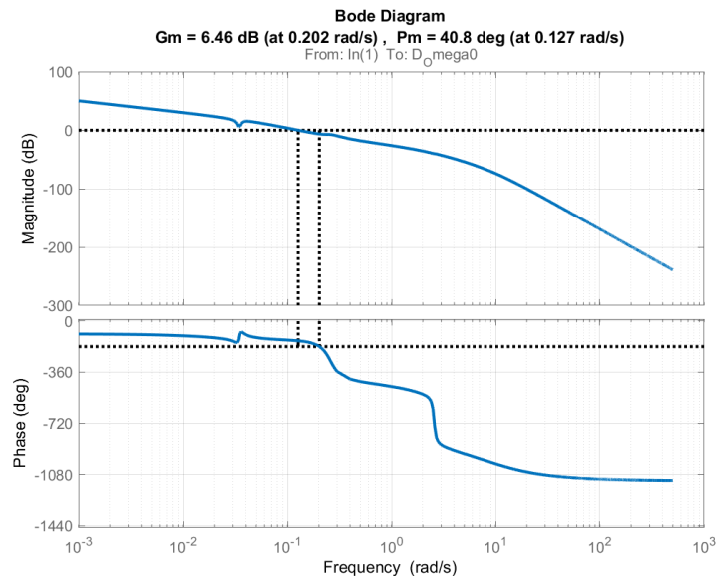


Figure 3-6: Bode plot showing stability margins for the open loop with CgLp. The bandwidth and phase margin are the same as the base linear system, but the gain margin has improved.

Comparing this open loop with the linear baseline, a better tracking performance is shown and a marginally improved bandwidth.

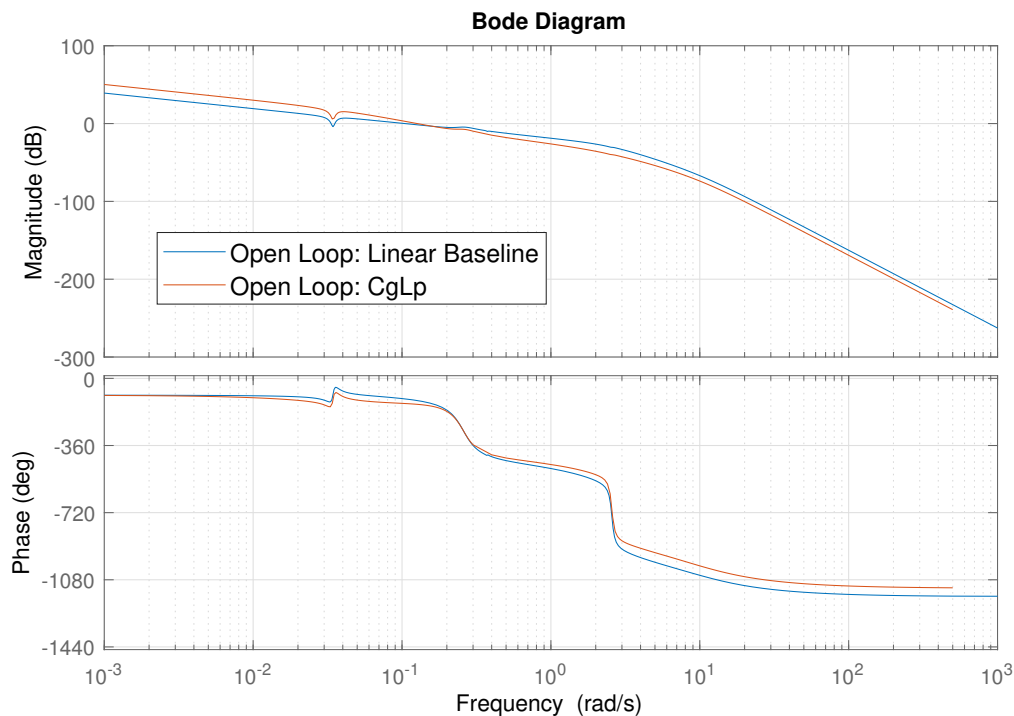


Figure 3-7: Bode plot comparing the open loop of the controller with CgLp to the linear baseline. Significant improvement is expected at low frequencies, especially the zeros at 0.034 rad/s corresponding to the surge motions of the platform. Also, a slightly better high frequency roll-off is seen.

When implementing the CgLp, another choice must be made. While in linear systems, the order of different elements (blocks in a block diagram) is irrelevant, that is not the case for non-linear systems. The outcome of controlling a system with a CgLp is heavily dependent on the order of the linear and non-linear elements. Both of these methods have advantages and disadvantages.

1. Reset Element - Lead Filter When the reset element comes first, the resets correspond to the zero crossings of the error signal. This is in line with the philosophy behind reset control: the control action changes when a target is reached to reduce overshoot. However, the resets are essentially discontinuities, and passing this signal through a lead filter leads to large peaks in the control signal. High frequency oscillations are introduced in the system. In some systems, this does not have to be a bad thing. The CgLp was originally applied to a precision positioning stage [1]. Here, the position of a small mass is controlled through voice coil actuators (an electrical actuator that generates linear motion). The input voltage for the actuator is the controlled variable. The maximum rate of change for the voltage does not pose a limiting factor for the performance of the system, so large peaks in the control signal are allowed. For the blades of a wind turbine however, it is near impossible as well as undesirable to make these rapid movements due to the large inertia of the components. Strictly speaking, the input voltage for the pitch motors can be viewed as the controlled variable, but as the

pitch motors are generally fast enough to track the pitch signal, it is not very useful to apply the CgLp there.

2. Lead Filter - Reset Element With the lead filter first, the resets can occur at irrelevant times, because the error signal first passes through the lead filter. Another disadvantage is that it is sensitive to noise. High frequency signals will increase in magnitude due to the lead filter, inducing resets at a high frequency. In any real world implementation, a solution for this behavior needs to be found. However, since the signal containing the resets will not go through the lead filter anymore, no extreme peaks in the signal will occur. Therefore, the extremely fast movements that occur in the first configuration do not occur here.

A quick comparison in the time domain (Figure 3-8) shows that method 1 is infeasible in combination with the controller in Figure 3-5. The large peaks in the control signal (blade pitch angle) are undesirable and lead to excitation of the fore-aft bending mode. Although the second method (seen in Figure 3-9) also shows jumps in the blade pitch, these are smaller in magnitude and don't induce high frequency oscillations.

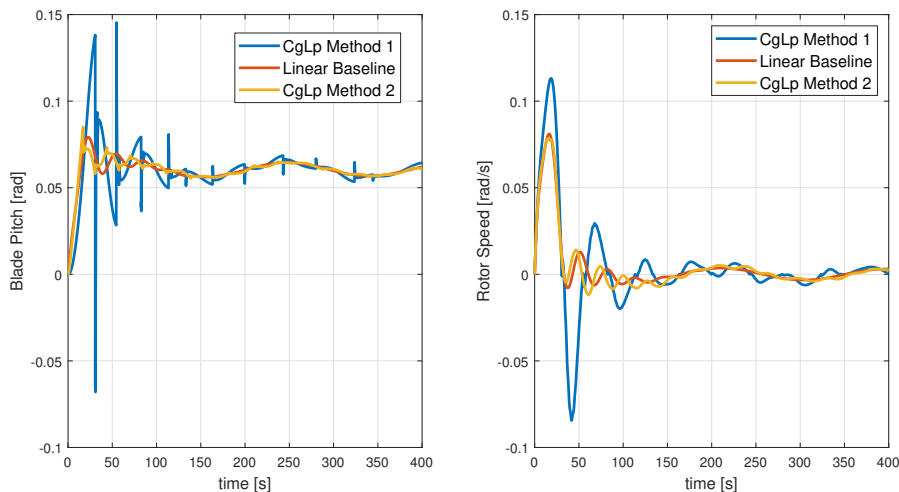


Figure 3-8: These graphs show the linearized wind turbine's response to a step in the windspeed. The blade pitch is shown on the left, and the rotor speed on the right. This figure shows the CgLp in both configurations as well as the linear baseline. Large peaks are shown in the blade pitch signal for method 1, over ten times as large as with the other method. Also, oscillations at the fore-aft tower bending mode's natural frequency show up in the rotor speed signal.

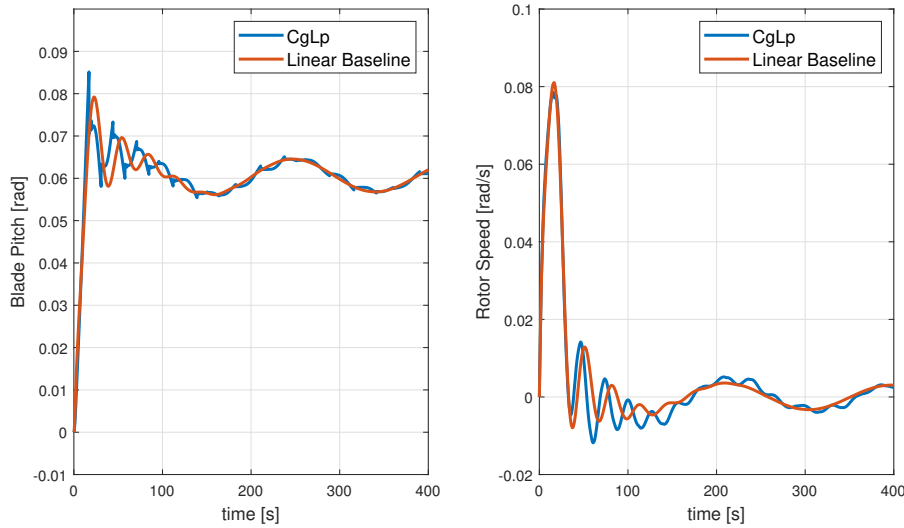


Figure 3-9: These graphs show the linearized wind turbine's response to a step in the windspeed. The blade pitch is shown on the left, and the rotor speed on the right. The graph shows the base linear system in orange and the CgLp in blue, where the order is like in method 2 (Lead Filter - SORE).

While the CgLp shows an improvement in tracking, gain margin and high frequency attenuation in the frequency domain (see Figure 3-4), these improvements are not obvious in the time domain simulation (see Figure 3-9). A slightly lower overshoot in the rotor speed is achieved, at the expense of much faster control inputs for the blade pitch. Also, the oscillations do not attenuate as fast, because the resets excite oscillations.

Second controller The first controller shows a clear improvement in the frequency domain, and a better performance is expected. However, it achieves no increase in bandwidth, so a second controller is tuned to see if it is possible to make a CgLp-based controller that is also faster than the baseline controller. A higher value of ω_r is selected to allow for a higher bandwidth. The second controller can also be tuned with a higher value of ω_f , to match the high frequency attenuation of the linear system. Then, after the CgLp is designed, the gains can be selected to achieve an increase in bandwidth with similar margins. The following parameters were selected:

$$\begin{array}{l|l} \lambda & 0.2 \\ \omega_r & 0.15 \\ \omega_f & 3 \\ \alpha & 1.04 \\ k_p & 0.363 \\ \omega_i & 0.275 \end{array}$$

This CgLp adds a phase of 31.4 degrees at the $\omega_r = 0.15$ radians per second, with a peak of 51.9 degrees at 0.48 radians per second. A comparison to the linear baseline is shown in Figure 3-10. Along with the PI controller, a bigger improvement in tracking performance is seen, and a higher bandwidth. Attenuation is only slightly better than the linear baseline,

as intended. However, the phase of this controller is lower at low frequencies, impacting performance at the frequency of surge motions.

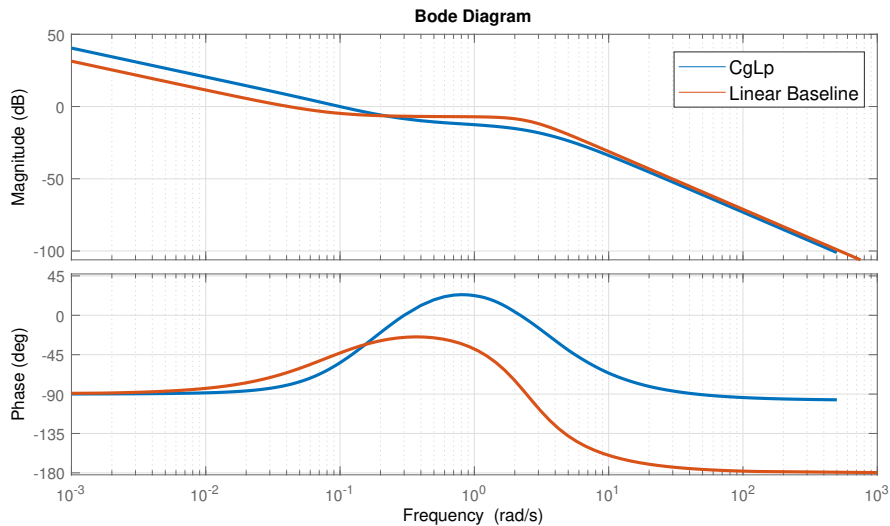


Figure 3-10: Bode plot of the second controller compared to the linear baseline.

The open loop is shown in Figure 3-11, which shows margins similar to the linear baseline, but with an increased bandwidth of 0.15 radians per second.

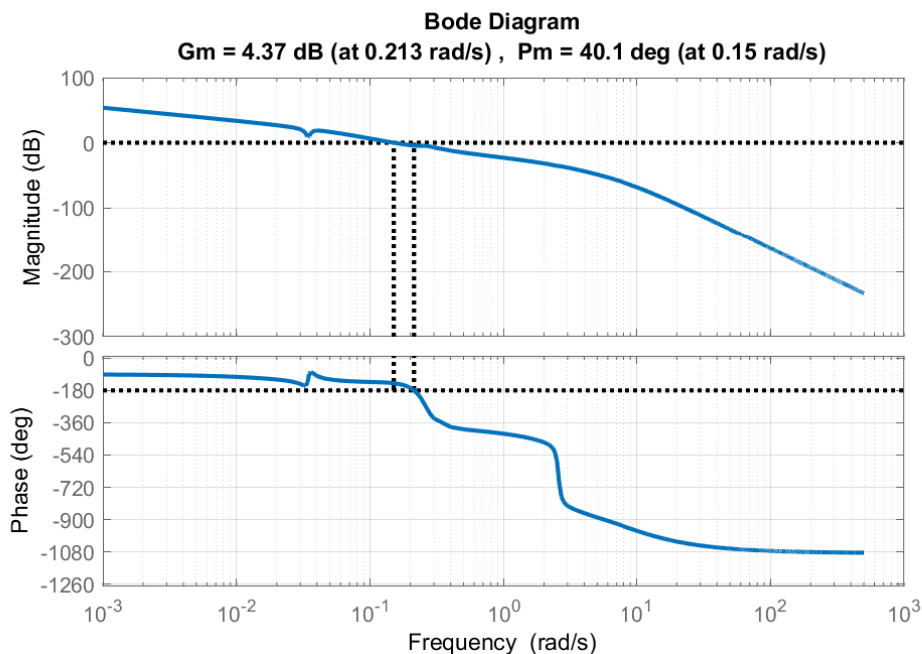


Figure 3-11: Open loop bode plot of the second controller with the FWT

Behavior in the time domain of this second controller is shown in Figure 3-12. A significant

reduction in overshoot is shown, at the cost of sustained oscillations at the platform pitch natural frequency.

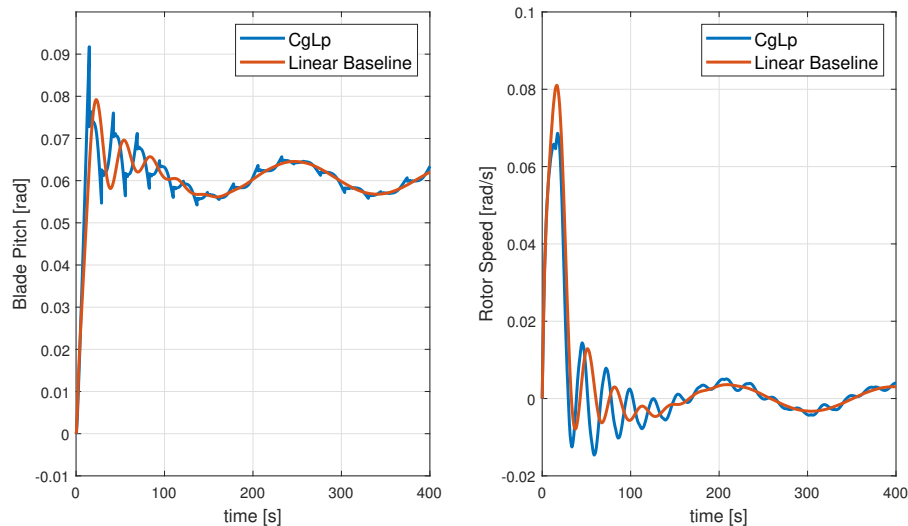


Figure 3-12: These graphs show the linearized wind turbine's response to a step in the windspeed. The blade pitch is shown on the left, and the rotor speed on the right. The graph shows the base linear system in orange and the CgLp in blue

In conclusion, this chapter discussed the design of two CgLp-based reset controllers. First, a linear model was introduced, along with a linear baseline controller. After that, the CgLp was selected as the most appropriate reset controller. It was determined that the original sequence of controller elements was unsuited for controlling a FWT due to the large peaks in the control signal. One controller was introduced with better stability margins and an increased gain at low frequencies. A second controller was introduced that has an increased bandwidth compared to the linear baseline. In the next chapter, simulations of the DTU 10MW FWT with the CgLp controller are shown, both with the linear model and the non-linear model in FAST.

Chapter 4

Results

In this chapter, various results of this thesis will be discussed. Different types of simulations were run, to discover the characteristics of the CgLp controller in combination with a floating wind turbine (FWT). The goal is first to view performance of the designed controller in various situations, to compare advantages and disadvantages. Secondly, robustness of the controller is reviewed. While no criteria to prove stability have been posed by the creators of the CgLp [1], it is shown that the behavior of the controller is stable even for large perturbations of the controller gains. Lastly, simulations in FAST are shown for a more accurate portrayal of a real floating wind turbine.

4-1 Simulation cases

Step The first type of simulation that is done is a step on the wind speed. In the case of a simulation with the linear model, the wind speed input is stepped up to 1 m/s from 0 m/s. Because it is a linearization of the FWT at steady state conditions at a wind speed of 12 m/s, this can be interpreted as a step from 12 m/s to 13 m/s.

For the simulation in FAST, this step is applied from 11.5 m/s to 12.5 m/s. This is done because the accuracy of the linear simulation decreases when the conditions divert from the 12 m/s steady state.

Also, the step is applied after 300 seconds of simulation. This is done to allow the FWT to settle to its steady state at 11.5 m/s, because it is difficult to perfectly set all the initial conditions to the steady state conditions.

NTM To test the controller and FWT under more realistic conditions, a turbulent wind according to IEC 61400-1 Normal Turbulence Model (NTM) is applied [56]. For the linearized model, the wind was averaged at 0 m/s, and in FAST the wind was averaged at 12 m/s. For the linear model, one single wind speed vector was used, as the model does not take into account differences in wind speed at different points on the rotor.

The controller was highly impaired by turbulent wind. This is mainly caused by the high frequency oscillations in the wind signal. Therefore, additional simulations were done where this high frequency content is reduced. For the linear system it was easy to filter the wind speed signal in Simulink. However, in FAST the wind speed is commanded through the S-Function and a filter could not be applied. Therefore, the rotor speed signal was filtered with the same filter before being used in the controller. Obviously this causes phase lag in the controller and the system characteristics such as bandwidth and stability margins are impacted by this filter.

While this is an entirely different simulation case, both for the linear and non-linear models, the inclusion of these simulation is motivated by the insights offered. While it is not realistic to have such winds, it is still much more realistic than a step in the wind, and it allows for a better understanding of the behavior of CgLp based controllers in combination with FWTs.

Robustness In order to see how the CgLp performs under uncertainty, the gains are adjusted. This was selected because it is simple to implement and there is already a lot of disturbance from the wind.

4-2 Linear Model

This section shows the simulation results of the linearized system.

Step Figure 4-1 shows a simulation of a step response of the first CgLp controller with the linearized FWT model. The main difference that is expected is improved behavior at low frequencies, especially at the frequency of platform surge motions. The simulation shows that at first, the resets introduce oscillations at the frequency of the platform pitch mode. This is undesired. After these oscillations have attenuated, around 500 seconds in, the expected increase in low frequency performance can be observed, as the rotor speed stays closer to its steady state value. However for the faster controller, seen in Figure 4-2, the oscillations induced by resets persist. While an even better low frequency disturbance rejection is expected, that is not observed in the step response.

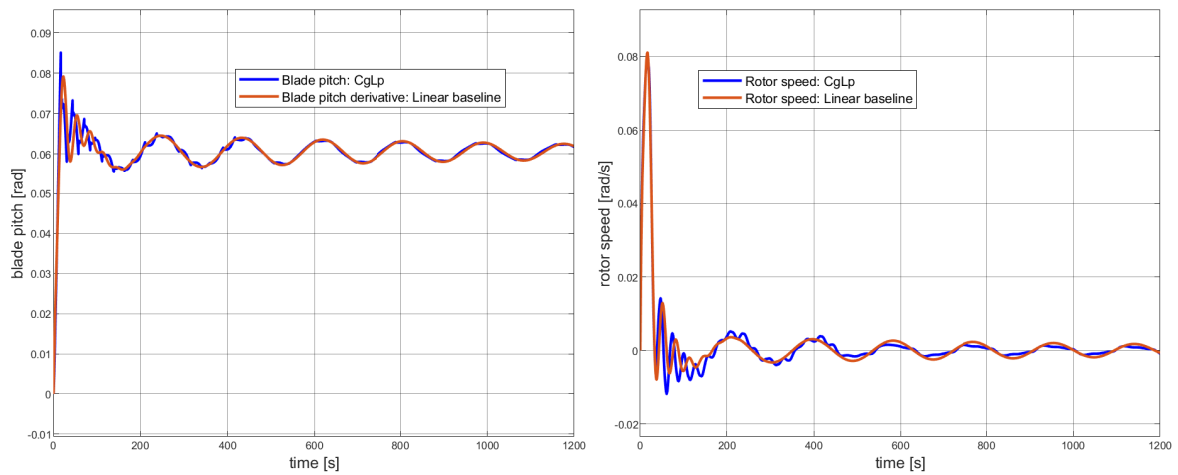


Figure 4-1: This figure shows an extended version of the simulations from the previous chapter with the first (slower) CgLp. It shows the FWTs behavior after a 1 m/s step on the wind speed. After the CgLp initially excited more oscillations at the platform pitch natural frequency, it shows a better rejection of the low frequency disturbance due to surge motions. This matches the frequency domain, where we see a higher gain at the zero pair corresponding to the surge motion.

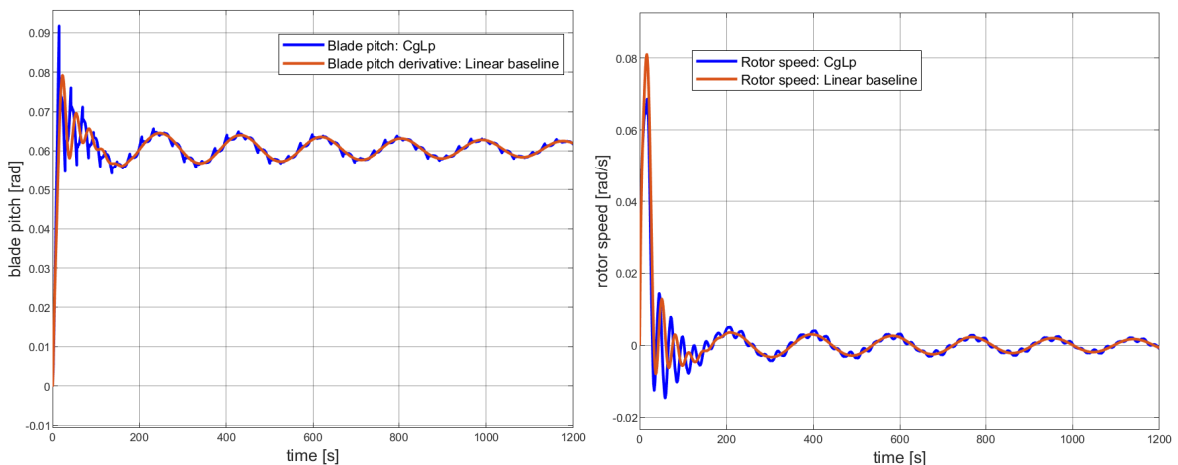


Figure 4-2: This figure shows an extended version of the simulations from the previous chapter with the second (faster) CgLp. It shows the FWTs behavior after a 1 m/s step on the wind speed. The frequency domain expectations do not hold here, as no improvement is seen because the oscillations at the platform pitch frequency continue throughout the simulation.

NTM Results with the second simulation case are shown here.

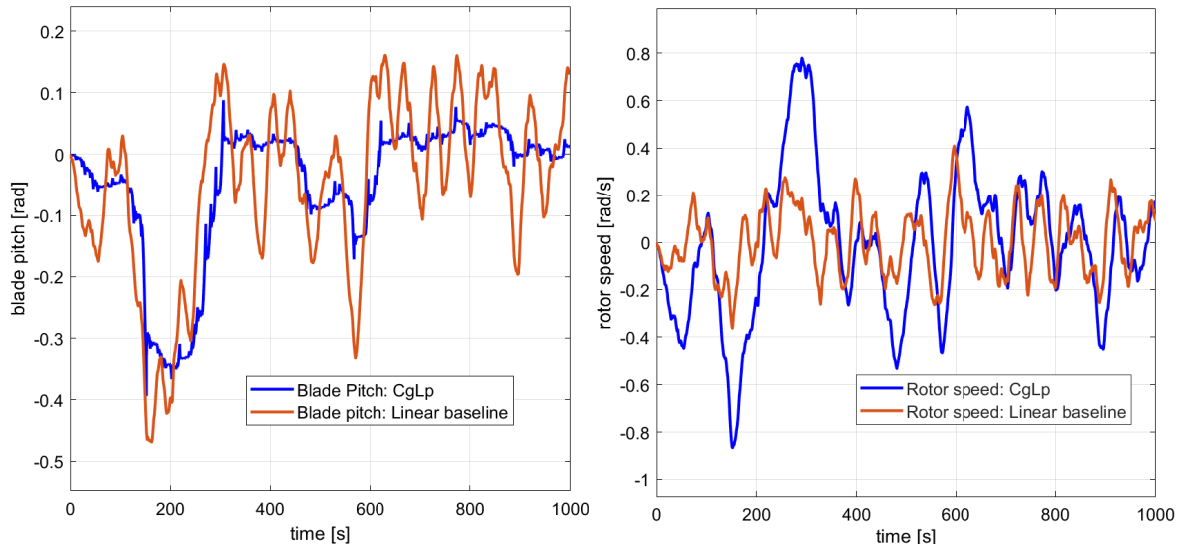


Figure 4-3: This figure shows the behavior of the linearized FWT model under turbulent wind. Clearly, the CgLP performs much worse, as there is much more variation in the rotor speed. The blade pitch does not seem to respond well compared to the linear baseline.

As the simulation in Figure 4-3 shows, the CgLP does not perform well under turbulent wind. Zoomed in on the first 50 seconds of the simulation, Figure 4-4 shows why: many resets occur in a short amount of time, when there is no advantage to these resets. The resets prevent the blade pitch from adjusting enough to keep the rotor speed close to its reference.

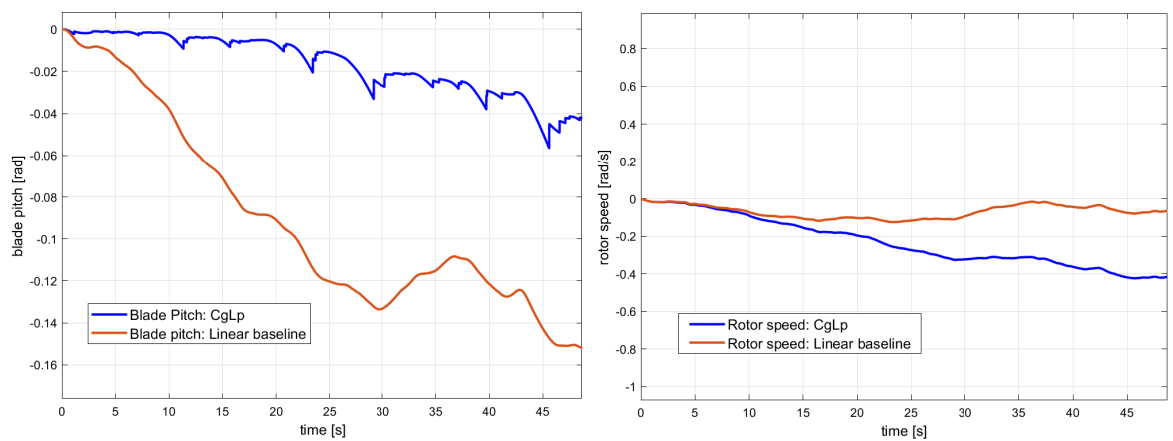


Figure 4-4: This figure shows the first 50 seconds of the simulation in Fig 4-3.

High frequency content in the wind signal translates to high frequencies in the rotor speed. This gets amplified by the lead filter, leading to zero crossings and hence highly frequent resets of the reset element.

To demonstrate the controller behavior in absence of excessive high frequencies, the disturbance (wind speed) is filtered first. This leads to the wind signal shown in Figure 4-5. As discussed at the introduction of the different simulation cases, this is not indicative of any real

world performance, and is solely intended to show the CgLps behavior with a more irregular signal than the step signal.

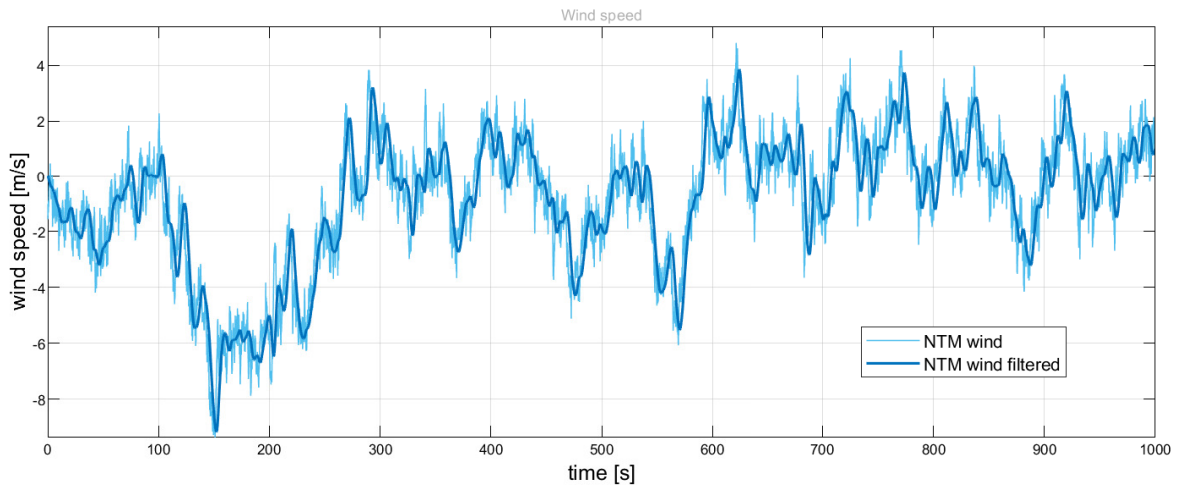


Figure 4-5: The filtered wind speed signal. A lowpass filter with corner frequency $\omega = 0.5$ rad/s is used. The signal is averaged at zero so that it can be used for the linearized model.

A simulation with this filtered disturbance is shown in Figure 4-6

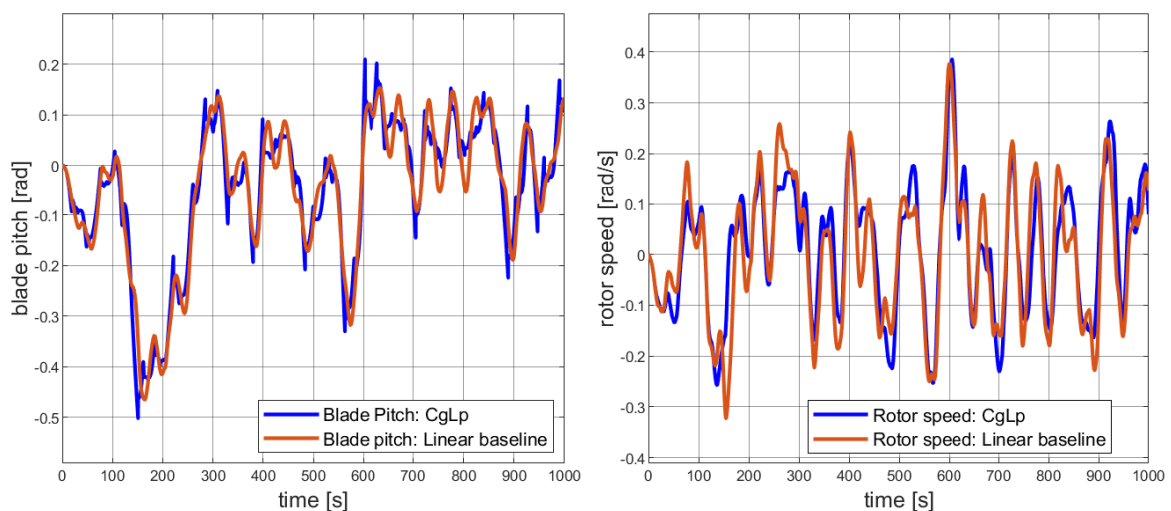


Figure 4-6: Simulation with filtered wind signal. The graph shows that the CgLp performance is quite similar to the linear performance. At some times, it clearly takes advantage of the phase lead over the linear controller, while at other times, the resets seem to delay the performance.

This simulation shows that the performance of the CgLp is much closer to the linear baseline in this case. The blade pitch signals stay quite close to each other. It can be seen that in some instances, the CgLp is much better at reducing the rotor speed error. For example, look at the behavior around between 250 and 300 seconds. At other times, the CgLp has a much higher peak, like between 450 and 550 seconds. This seems a bit unreliable and it is

hard to tell from the graph whether performance has increased. For a numerical analysis of performance, let us look at the root mean square error of the rotor speed in Table 4-1.

	NTM	NTM Filtered
Linear Baseline	0.1408 rad/s	0.1344 rad/s
CgLp	0.2919 rad/s	0.1270 rad/s

Table 4-1: RMS error for the CgLp and linear baseline controller in simulations with NTM and the filtered wind speed. The CgLp performs better than the linear controller when the wind input does not contain high frequencies.

These results are closer to what is expected based on the step result and frequency domain behaviour of the CgLp. However, the viability of this design also depends on the pitch actions. These are shown in Figure 4-7.

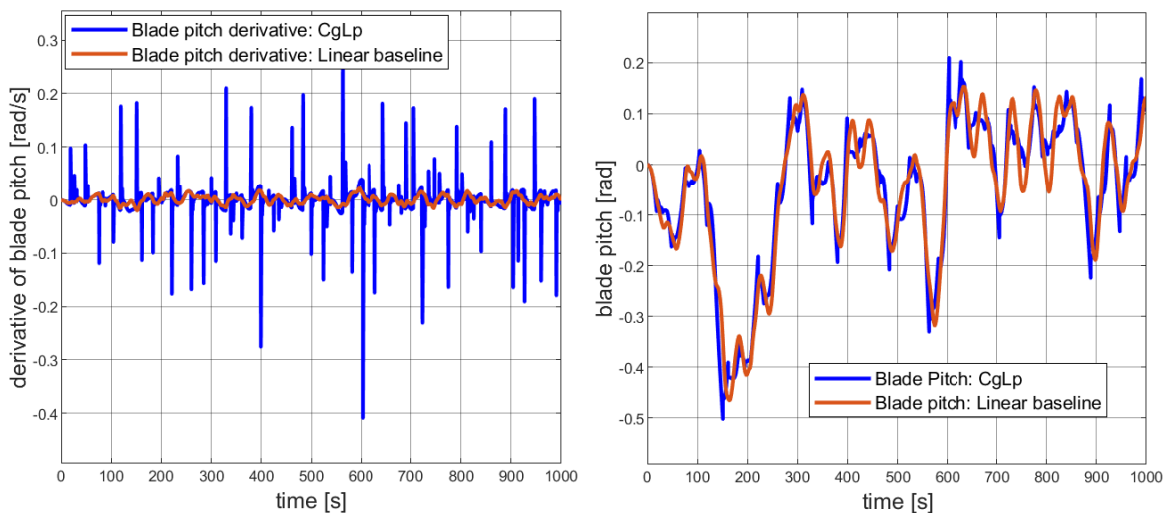


Figure 4-7: Simulation with filtered wind signal. While the blade pitch signals seem quite similar, the derivative (pitching speed) tells a different story. Large peaks are shown for the CgLp, so the pitch motors are working very rapidly.

This large difference in the speed that is demanded from the pitch motors signals a trade-off. These pitch motions will put a lot of strain on many of the machines parts and this will only be worth it when there is a large increase in performance with respect to the rotor speed.

Summarizing the results so far, the step response showed an expected performance from the first CgLp, but a disappointing performance from the more aggressive CgLp, because the resets induce excessive oscillations at the platform pitch natural frequency. Under turbulent wind, the performance from the CgLp completely broke down. When high frequency content is not present in the wind signal, the performance is closer to the expected performance, but a bit unreliable. However, when looking at the blade pitch actions, it is clear that the trade-off is likely not worth it: the blades pitch at a much higher rate than in the linear baseline and the increase in performance is marginal and unreliable.

Robustness Another interesting aspect of the CgLp controller is robustness. As mentioned in Chapter 2-5, stability of reset controllers is never obvious. It is not guaranteed by having a stable base linear system, nor by a describing function with sufficient stability margins. While this thesis is not focused on the theoretical details of stability for reset controllers, a quick test was done to check the behavior. The controller gains are increased by a certain percentage to see how easily the controller is destabilized. The results are shown in Figure 4-8.

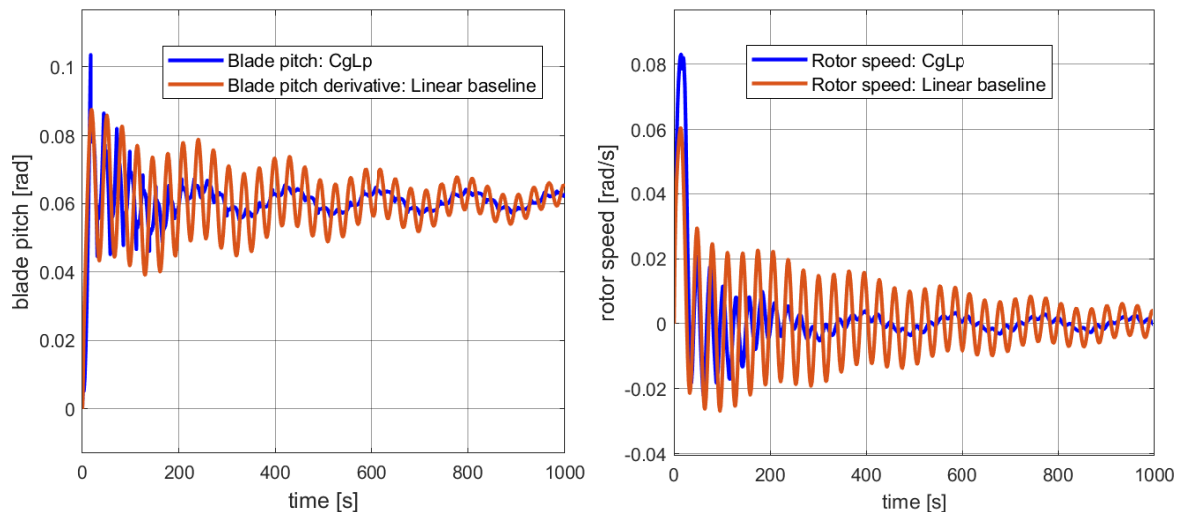


Figure 4-8: Step response with an increased loop gain by 60%. The linear baseline is barely stable, but the CgLp shows similar behavior to the normal gains. For this design, the gain margin is 0.23 dB and the phase margin is 5.35 degrees. Therefore, the response dampens out much quicker than expected.

This shows a remarkable property of the CgLp. While the linear baseline is pushed towards the edge of instability, increasing the CgLp loop gain by 60% seems to have a minor impact. It even seems to perform more slowly, due to an unnecessary reset that already happens before the 3 second mark, as shown in Figure 4-9. While it seems positive that there is no big risk of destabilizing the system with the CgLp, it also shows that the frequency domain information can not give accurate predictions for time domain performance.

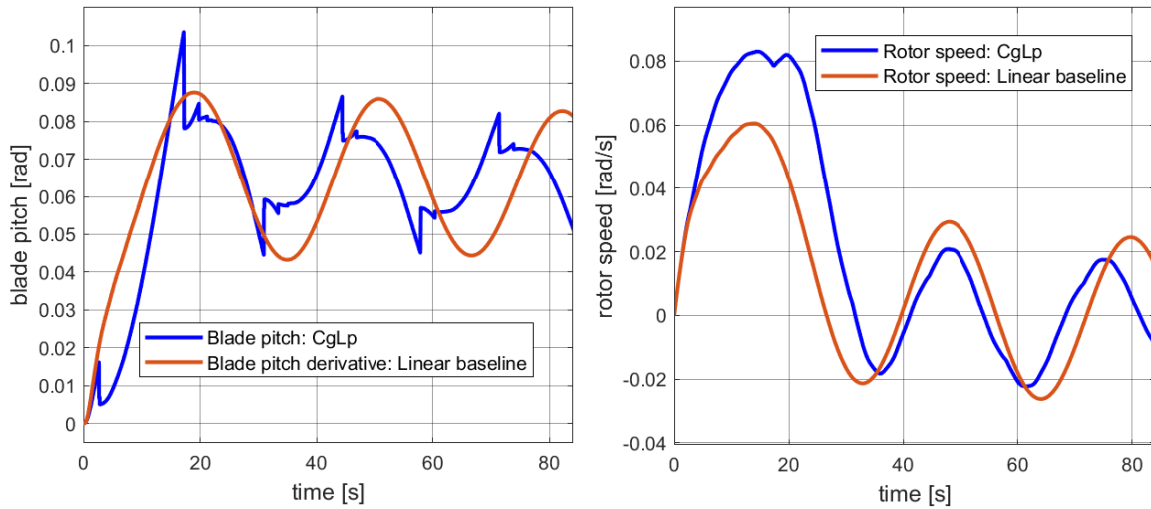


Figure 4-9: The simulation from Figure 4-8, zoomed in on the first 80 seconds.

So while the risk of instability is not as big, performance of the CgLp in this application is not very reliable. Figure 4-10 shows how even a small increase of the gain (3%) can impact performance a lot.

This also shows that the controller gains do not have a very large impact on the performance of the CgLp (in this configuration) after a certain point. While low gains can still make the system slow, very high gains do not change much. The corner frequencies of the CgLp are the main parameters when it comes to the time domain performance of the system.

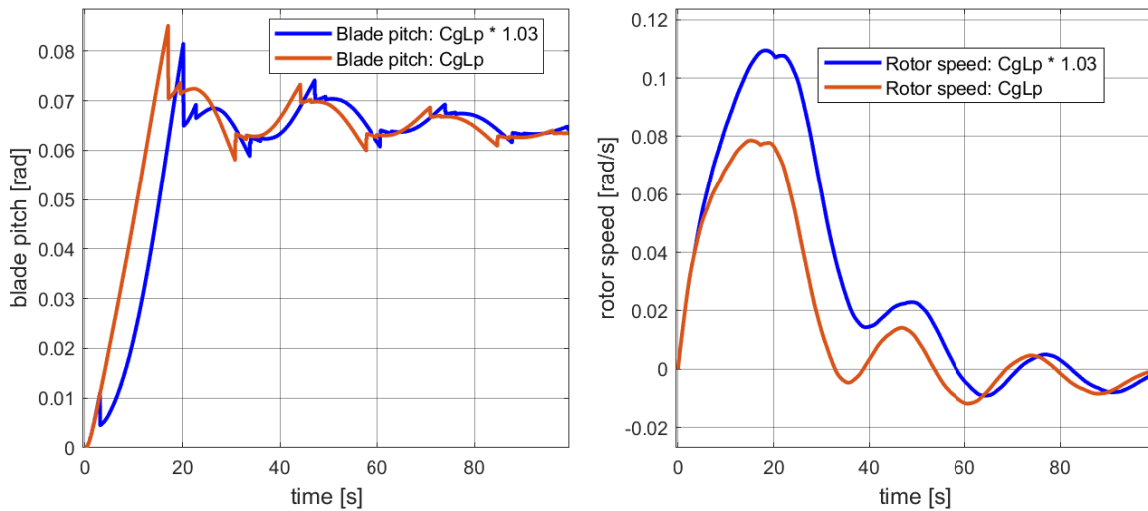


Figure 4-10: Simulation of Two CgLp's with the FWT, where one has the loop gain increased by 3%. This increased gain actually seems to make the performance slower due to a badly timed reset.

In conclusion, while there are no guarantees for stability, the CgLp seems to remain stable both under turbulent disturbance and uncertainty in the loop gains. Even large increases in

the gain do not destabilize the system. However, it is shown that the performance of the CgLp is hard to predict. This raises questions about the accuracy of the step response as a proxy for all-round performance for non-linear systems, as a small perturbation in the system leads to wildly different response. Also, neither the step response nor the bode plot can predict the bad performance under turbulent winds.

4-3 Non-linear simulations in FAST

Fatigue, Aerodynamics, Structures, and Turbulence (FAST) is a high fidelity simulation tool, allowing for non-linear simulations of the FWT introduced in Section 2-4. A step response of the non-linear FWT is shown in Figure 4-11. A step from 11.5 to 12.5 m/s was selected, as the design is based on the linearization at 12 m/s, and that is also the most critical wind speed for the negative aerodynamic damping. Also, while the original gain scheduling is still active for the CgLp, it has not been confirmed that the same gain scheduling is appropriate for use with the CgLp. Therefore, to get more accurate results, the choice was made to stay close to the linearization point.

These figures show simulations starting after 200 or 300 seconds to give the system time to reach a steady state, as this was easier than perfectly setting every initial value for the simulation. For the step response, the system has completely settled after 300 seconds. For the turbulent simulations, the simulation starts at 200 seconds. The responses of the different simulations are not settled at this time due to the turbulent wind, but the effect of the initial conditions on the simulation is very small at this point in time.

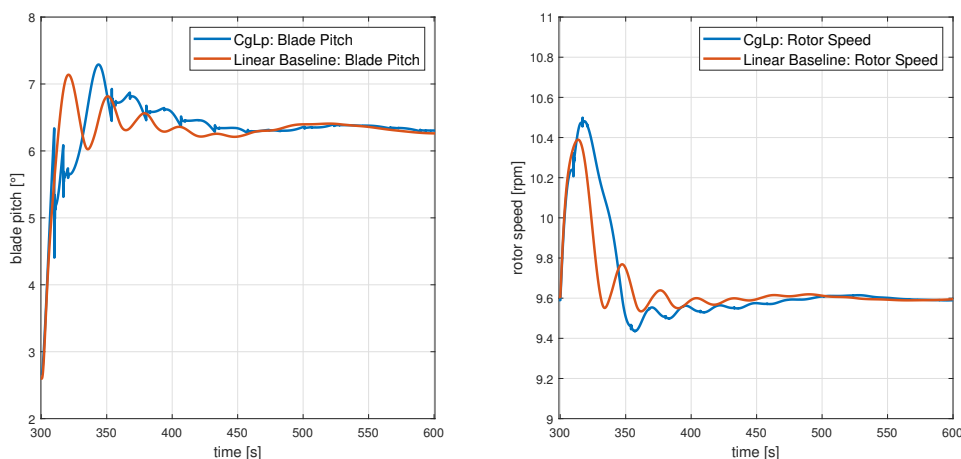


Figure 4-11: Simulation with FAST of a step in the wind, (from 11.5 to 12.5 m/s) with the CgLp and the linear baseline controller. A reset is also shown when the blade pitch was still rising towards the value it settles at, making its performance worse compared to the linear baseline.

Here, the unreliable performance of the CgLp is shown again. It was already shown in Figure 4-10 that a small deviation from the designed controller could give undesired resets. Here, a deviation in the plant is present (from a linearization to the non-linear model), leading to a worsened behavior. The decreased performance is again caused by a premature

reset. The reason that this happens is uncertain, but several non-linear dynamics exist in the wind turbine that might induce high frequencies in the rotor speed signal. For example, the linearized model does not contain a model for elastic behavior of each blade separately, while they might still oscillate.

In Figure 4-12, a simulation with turbulent wind is shown (NTM). Behavior is similar to the linear model with turbulent wind: the high frequencies in the rotor speed signal cause excessive resets. The blade pitch is prevented from adjusting to different wind speeds, and therefore, the rotor speed has large variations.

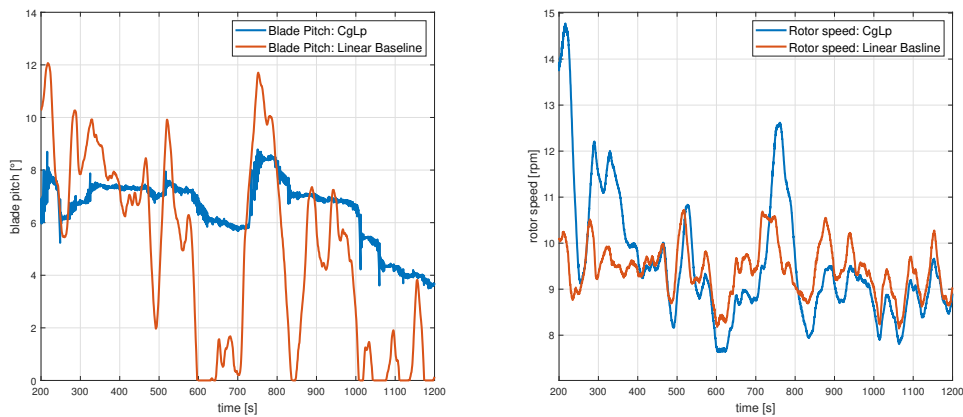


Figure 4-12: Simulation with FAST with turbulent wind, (averaged at 12 m/s) with the CgLp and the linear baseline controller. Excessive resets can be seen in the blade pitch signal of the CgLp.

As explained in Section 4-1, it is more difficult to filter the wind speed in FAST. Therefore, the rotor speed is filtered instead. The same filter is used that the linear baseline uses. Remember, for the CgLp, this filter should not be necessary because in the bode plot of the CgLp, low pass characteristics are already present. Therefore, including this filter will only slow down the response, negating (at least partly) the advantages that reset control can offer. Figure 4-13 compares the step responses of the CgLp without a filter and with a filter. The premature reset seen in the unfiltered CgLp does not occur for the filtered CgLp. Its performance is very similar to the linear baseline. However, the disadvantage of the spikes in the blade pitch signal are still present, so the CgLp is not preferred.

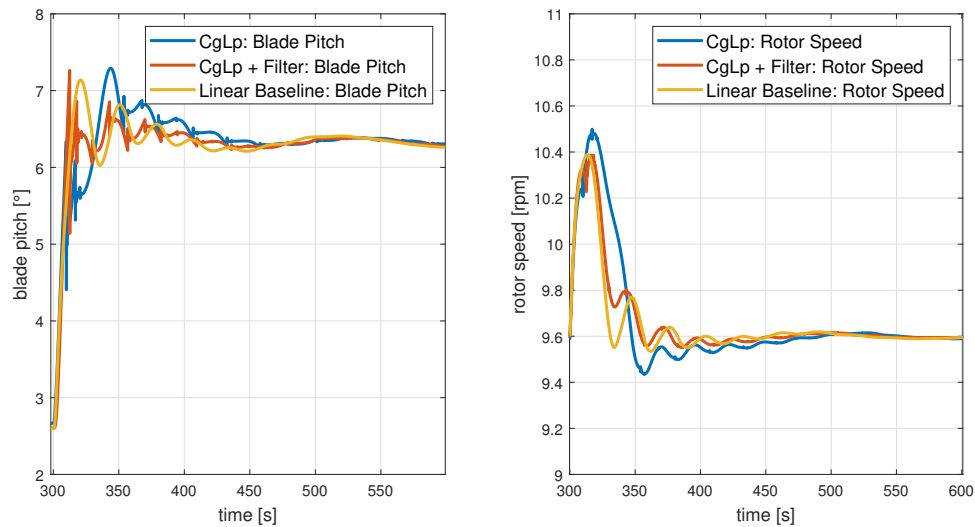


Figure 4-13: Simulation with FAST of a step in the wind, (from 11.5 to 12.5 m/s) with the CgLp and the CgLp with filter. An improvement is shown because the filtered CgLp avoids resetting too soon. A similar overshoot as the linear baseline can be seen, and the phase advantage of the CgLp still shows (the oscillations are shifted to the left compared to the linear baseline.)

Combining this filtered CgLp with turbulent wind, as seen in Figure 4-14, yields better results than the unfiltered CgLp. The controller does not reset as much, allowing the blade pitch to adjust. The rotor speed is much closer to the rotor speed observed for the linear baseline, but it still achieves a lower performance, with a higher RMS error and a higher maximum error.

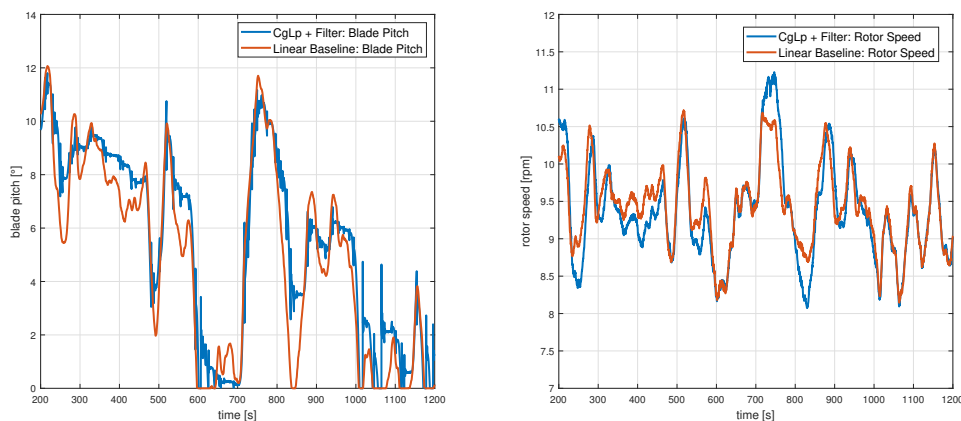


Figure 4-14: Simulation with FAST of turbulent wind (averaged at 12 m/s) with the CgLp with filter compared to the Linear baseline. The CgLp's performance is much better with a filtered rotor speed signal. However, it still does not perform as well as the linear controller. The RMS error of the CgLp is 0.71 rpm, while the RMS error of the linear baseline is 0.59 rpm.

This chapter has shown the designed controller in different circumstances. Idealized conditions, such as a step on the wind or a smoothed turbulent disturbance, show an expected

performance: a slight increase in performance (variation of the rotor speed) over the linear baseline can be seen in these simulations, but the disadvantages of the resets are also clear. However, in other simulations, it becomes instantly clear that the CgLp is not suitable for implementation in FWTs. It is shown that small differences (a small adjustment to the loop gain, or a more complex model) already deteriorate the performance. The biggest problem however, is that high frequencies in the error signal completely inhibit the controller from producing adequate responses to disturbances. The next chapter talks about the lessons that can be learned from these results.

Chapter 5

Conclusion

Man-made climate change has given us an increased demand for renewable power, and floating wind turbines (FWTs) can be an important piece in the puzzle. Currently, the control performance of FWTs is limited by the problem of negative aerodynamic damping, represented by right half-plane (RHP) zeros in the system model. Some of the proposed solutions for this problem have been discussed, but they all come with disadvantages too. This thesis set out to solve this problem, with the following research statement:

Investigate possibilities to increase the control performance of FWTs based on advanced reset controllers.

A general conclusion that can be made is that the results shown in Chapter 4 are not overwhelmingly positive. The promising characteristics discussed in Chapter 2, nor the promising frequency domain plots in Chapter 3 seem to translate to positive results in the simulations of Chapter 4. Therefore, it can be concluded that the control performance of FWTs can likely not be improved by reset controllers. However, some additional conclusions can be drawn from what is shown in the results.

5-1 Sub-objectives

The first sub-objective in the research statement is the following:

Deliberately select a controller architecture that is most suitable for implementation with FWT and tune it for a specific FWT model

The CgLp was selected as a controller architecture. This was motivated by the fact that it is capable of adding phase where it counts: around the RHP zeroes. Based on the open loop bode plots presented in Chapter 3, this was the right decision. An alteration to the original CgLp controller, presented in [1], was made. The order of the non-linear and linear elements was swapped around for implementation in FWTs. This led to the following conclusions about the CgLp:

In the frequency domain, a theoretical improvement in performance is observed. This is based on the bode plot of the open loop system, where the describing function is used for the CgLp. As expected, the bandwidth is still limited by the RHP zeroes. Therefore, there is only a minor increase in performance as measured by the bandwidth and stability margins.

The CgLp in the original order (Reset Element - Lead Filter) causes large peaks in the output. When the reset element comes first, a signal with jumps will pass through the lead filter. According to the Fourier transform, such a jump consists of many higher order sinuses with high frequencies. The lead filter amplifies high frequencies, leading to peaks in the control signal. This is the reason that this configuration was not chosen for the FWT: the control signal is the blade pitch, and such large movements are undesired for heavy components such as the blade of a 10 MW wind turbine. In other applications, where the control variable lends itself better to these large peaks, this is not always a problem.

The second sub-objective is:

Perform simulations comparing the reset based controller to a baseline controller, to review the performance of reset control for FWT

Based on the simulations, the following conclusions can be drawn:

The CgLp, with the linear element and reset element in reverse order, causes a deteriorated performance in presence of high frequency content in the input signal. The high frequencies in the error signal, which might be present due to noise or high frequency disturbance, get amplified by the lead filter. This leads to many zero crossings, which will trigger the reset condition of the second-order reset element (SORE). Therefore, the output of the SORE stays limited, and the controller output can not increase sufficiently to deal with disturbances.

The reason that system behavior deviates so far from what is expected based on the describing function, is that this large impact of high frequencies on the system behavior can not be seen in the frequency domain. In Figure 4-4, it is shown that resets can occur each second or even more frequently. However, the open loop bode plot of the system in Figure 3-11 shows that 1 Hz (6.28 rad/s) signals should be filtered out with -60 dB. These resets have a large impact on the slower behavior that should dominate, not by directly propagating in the system but by 'jamming' these control actions. Therefore, the describing function is not an adequate representation of the non-linear controller in this case, even though it seemed accurate in simulations without high frequency disturbances. The conclusion is that this will likely cause problems in most real world use cases.

With an ideal (smooth) disturbance signal, the CgLp can lead to increased disturbance rejection performance for FWT. The higher bandwidth that is observed in the open loop bode plot of the system with CgLp controller can also be observed under certain ideal circumstances. This results in a lower root mean square (RMS) error of the rotor speed signal in simulations on the linearized system. However, these conditions are idealized and unrealistic. Also, this result is partly based on randomness, as the performance is better during some parts of the simulation, but not during all parts.

The control signal for the CgLp is much more irregular than the linear baseline. Rapid movements of the rotor blades are observed during simulations of the FWT with the CgLp based controller. Even under the idealized conditions, this would put large loads on the turbine's structure and on the pitch motors. Even if the CgLp would lead to an increased performance for rotor disturbance rejection in most real world cases, the advantage will likely not outweigh the costs associated with these loads. These rapid movements severely increase fatigue forces on the blades and turbine structure, and introduce much more wear on the pitch motors (or it may even require much stronger pitch motors). While this thesis does not include a cost-benefit analysis, it is likely that using the CgLp as a cost-effective solution for the problems associated with RHP zeroes is not feasible.

The performance of a CgLp for a FWT in turbulent wind (according to the Normal Turbulence Model (NTM)) is worse than the linear baseline. In these conditions, high frequency oscillations are present in the rotor speed signal due to the turbulent wind. As discussed in the previous section, this leads to excessive resets of the SORE. Therefore, the CgLp is unfeasible for implementation on a FWT.

In summary, this thesis aimed to research the possibilities of advanced reset controllers for application in the control of floating wind turbines. The CgLp had the most potential for this application. A CgLp based controller was designed and simulations on both a linearized model and a non-linear model of a 10MW reference FWT were done. These simulations led to the conclusion that reset technology is not suitable for this application.

Discussion and Recommendations

This chapter discusses the work in this thesis and gives recommendations for future research.

Firstly, the results show that reset control is not as promising as it seemed. It is still possible that a different approach would have given better results. Some of the design choices that have been made, while they were well thought out, may have been less than optimal. However, this thesis still reveals the characteristics of the CgLp in combination with a floating wind turbine (FWT), which are unfavorable. Therefore, it is unlikely that a different approach would lead to a different conclusion.

Despite this, it could have been more interesting to use the original controller structure of the CgLp (Reset Element - Lead Filter). While it will likely be bad for a real FWT due to the peaks in the controlled variable, it may have been insightful to see the potential of this technology in systems with RHP zeros. Future research could look into this problem, but it might be more recommendable to select another system with RHP zeros and a control variable that is not negatively impacted by these large peaks.

It may have been interesting as well to consider more advanced types of reset controllers. While this thesis aimed to find a controller that could easily be implemented in a normal SISO feedback controller, more complex controllers that rely on more computational power may perform better. An example of this would be a robust reset controller with an adaptive feedforward gain [52].

Another consideration is that while the design was mainly guided by frequency domain tools, the time domain tools were also used for validation, making the process iterative. It is possible that an approach that relies more heavily on time domain results, while less systematic, could give better results with the original controller structure, since the main concern with that structure is the peaks of the controller signal observed in the time domain. More design tools such as higher-order sinusoidal input describing function (HOSIDF) [57] can also be applied to gain more insight into the undesired behaviours of reset elements.

A different thing that may be worthwhile to research is a way to solve the excessive resets in the CgLp in the configuration that this thesis used. It is shown in the results that filtering the error signal will reduce this effect, but the phase loss of the filter negates the phase advantage

of the CgLp. If an optimum can be found where the controller still takes advantage of the increase in phase while preventing the excessive resets, performance can still be increased.

While the CgLp has proven to be unsuccessful in pitch control for FWTs, this does not necessarily mean that there is no application for reset control in the broader field of wind turbine control. Keeping in mind the limitations discussed in Chapter 5, a new application might be found in wind turbines. For example, generator torque is not as constrained by inertia, so the CgLp may succeed in torque control.

To increase the performance of FWTs, other controllers are better suited. An interesting approach for future research may be to combine some of the controllers that were mentioned in 2. For example, parallel path modification (as seen in [9]), can be used alongside the adjusted robust gain scheduling from [8]. The first solution aims at improving the performance at a specific operating point, while the second solution tries to optimize the performance at each operating point. This robust gain scheduling method may be a key for implementing different kinds of future controllers.

Lastly, a lot of research is being done in the field of reset control. As progress in the field continues, future reset controllers may be better suited for application in FWTs.

Appendix A

Linearized Model

This Appendix gives the state space matrices of the linearization from SLOW at a wind speed of 12 m/s [15].

$$B = \begin{bmatrix} 0 & 0 & 0 & 0 & 0 & 0 \\ 0 & 0 & 0 & 0 & 0 & 0 \\ 0 & 0 & 0 & 0 & 0 & 0 \\ 0 & 0 & 0 & 0 & 0 & 0 \\ 0 & 0 & 0 & 0 & 0 & 0 \\ 0 & 0 & -2.922*10^{-4} & 4.969*10^{-8} & -1.326*10^{-9} & 1.031*10^{-9} \\ 0 & 0 & -4.245*10^{-4} & -1.315*10^{-9} & 2.611*10^{-8} & -4.221*10^{-11} \\ 0 & 0 & -7.176*10^{-6} & 1.022*10^{-9} & -4.221*10^{-11} & 3.307*10^{-11} \\ -3.125e-07 & 0 & 0.01568 & 0 & 0 & 0 \\ 0 & 0 & 0.1949 & -1.636*10^{-7} & 6.737*10^{-9} & -4.736*10^{-9} \\ 0 & 101.1 & 0 & 0 & 0 & 0 \end{bmatrix} \quad (\text{A-1})$$

$$C = \begin{bmatrix} 1 & 0 & 0 & 0 & 0 & 0 & 0 & 0 & 0 & 0 & 0 \\ 0 & 1 & 0 & 0 & 0 & 0 & 0 & 0 & 0 & 0 & 0 \\ 0 & 0 & 1 & 0 & 0 & 0 & 0 & 0 & 0 & 0 & 0 \\ 0 & 0 & 0 & 1 & 0 & 0 & 0 & 0 & 0 & 0 & 0 \\ 0 & 0 & 0 & 0 & 1 & 0 & 0 & 0 & 0 & 0 & 0 \\ 0 & 0 & 0 & 0 & 0 & 1 & 0 & 0 & 0 & 0 & 0 \\ 0 & 0 & 0 & 0 & 0 & 0 & 1 & 0 & 0 & 0 & 0 \\ 0 & 0 & 0 & 0 & 0 & 0 & 0 & 1 & 0 & 0 & 0 \\ 0 & 0 & 0 & 0 & 0 & 0 & 0 & 0 & 1 & 0 & 0 \\ 0 & 0 & 0 & 0 & 0 & 0 & 0 & 0 & 0 & 1 & 0 \\ 0 & 0 & 0 & 0 & 0 & 0 & 0 & 0 & 0 & 0 & 1 \end{bmatrix} \quad (\text{A-2})$$

$$D = \begin{bmatrix} 0 & 0 & 0 & 0 & 0 & 0 \\ 0 & 0 & 0 & 0 & 0 & 0 \\ 0 & 0 & 0 & 0 & 0 & 0 \\ 0 & 0 & 0 & 0 & 0 & 0 \\ 0 & 0 & 0 & 0 & 0 & 0 \\ 0 & 0 & 0 & 0 & 0 & 0 \\ 0 & 0 & 0 & 0 & 0 & 0 \\ 0 & 0 & 0 & 0 & 0 & 0 \\ 0 & 0 & 0 & 0 & 0 & 0 \\ 0 & 0 & 0 & 0 & 0 & 0 \\ 0 & 0 & 0 & 0 & 0 & 0 \end{bmatrix} \quad (\text{A-3})$$

Bibliography

- [1] N. Saikumar, R. K. Sinha, and S. H. HosseinNia, "'Constant in gain Lead in phase' element - Application in precision motion control," 5 2018.
- [2] E. A. Bossanyi, "The Design of closed loop controllers for wind turbines," *Wind Energy*, 2000.
- [3] D. Kallehave, B. W. Byrne, C. LeBlanc Thilsted, and K. K. Mikkelsen, "Optimization of monopiles for offshore wind turbines," *Philosophical Transactions of the Royal Society A: Mathematical, Physical and Engineering Sciences*, vol. 373, 2 2015.
- [4] W. Heronemus, "Power from the offshore winds," *University of Massachusetts, Department of Civil Engineering, 8th Annual Conference and Exposition Marine Technology Society, Washington DC, USA*, 1972.
- [5] S. Butterfield, W. Musial, J. Jonkman, P. Sclavounos, and L. Wayman, "Engineering Challenges for Floating Offshore Wind Turbines," 11 2006.
- [6] B. H. Bulder, M. T. Van Hees, A. Henderson, R. H. M. Huijsmans, J. T. G. Pierik, E. J. B. Snijders, G. H. Wijnants, and M. J. Wolf, "Study to feasibility of and boundary conditions for floating offshore wind turbines," *ECN, MARIN, Lagerway the Windmaster, TNO, TUD, Technical Report*, vol. 43, 2002.
- [7] T. J. Larsen and T. D. Hanson, "A method to avoid negative damped low frequent tower vibrations for a floating, pitch controlled wind turbine," *Journal of Physics: Conference Series*, vol. 75, p. 012073, 7 2007.
- [8] F. Lemmer, W. Yu, D. Schlipf, and P. W. Cheng, "Robust gain scheduling baseline controller for floating offshore wind turbines," *Wind Energy*, p. we.2408, 9 2019.
- [9] B. Fischer, "Reducing rotor speed variations of floating wind turbines by compensation of non-minimum phase zeros," *IET Renewable Power Generation*, vol. 7, pp. 413–419, 7 2013.
- [10] A. Baños and A. Barreiro, *Reset Control Systems*. 2012.

- [11] A. Baños and A. Vidal, “Definition and tuning of a PI+ CI reset controller,” in *European Control Conference (ECC)*, 2007.
- [12] A. Baños, S. Dormido, and A. Barreiro, “Limit cycles analysis of reset control systems with reset band,” *Nonlinear Analysis: Hybrid Systems*, vol. 5, pp. 163–173, 5 2011.
- [13] D. A. Deenen, M. F. Heertjes, W. P. Heemels, and H. Nijmeijer, “Hybrid integrator design for enhanced tracking in motion control,” in *Proceedings of the American Control Conference*, 2017.
- [14] M. Heertjes, N. Irigoyen, and D. Deenen, “Data-driven tuning of a hybrid integrator-gain system,” *IFAC-PapersOnLine*, 2017.
- [15] F. Lemmer, “Low-order modeling, controller design and optimization of floating offshore wind turbines,” 2018.
- [16] R. K. Pachauri, M. R. Allen, V. R. Barros, J. Broome, W. Cramer, R. Christ, J. A. Church, L. Clarke, Q. Dahe, P. Dasgupta, and others, *Climate change 2014: synthesis report. Contribution of Working Groups I, II and III to the fifth assessment report of the Intergovernmental Panel on Climate Change*. IPCC, 2014.
- [17] X. Lu, M. B. McElroy, and J. Kiviluoma, “Global potential for wind-generated electricity,” *Proceedings of the National Academy of Sciences of the United States of America*, vol. 106, pp. 10933–10938, 7 2009.
- [18] M. A. Petrova, “NIMBYism revisited: public acceptance of wind energy in the United States,” *Wiley Interdisciplinary Reviews: Climate Change*, vol. 4, pp. 575–601, 11 2013.
- [19] X. Wang, X. Zeng, J. Li, X. Yang, and H. Wang, “A review on recent advancements of substructures for offshore wind turbines,” *Energy Conversion and Management*, vol. 158, pp. 103–119, 2 2018.
- [20] C. M. Wang, T. Utsunomiya, S. C. Wee, and Y. S. Choo, “Research on floating wind turbines: a literature survey,” *The IES Journal Part A: Civil & Structural Engineering*, vol. 3, pp. 267–277, 11 2010.
- [21] Matthew Hannon, Eva Topham, James Dixon, David Mcmillan, and Maurizio Collu, “Offshore wind, ready to float? Global and UK trends in the floating offshore wind market,” 2019.
- [22] J. M. Jonkman, “Dynamics Modeling and Loads Analysis of an Offshore Floating Wind Turbine,” 1 2007.
- [23] J. C. Clegg, “A nonlinear integrator for servomechanisms,” *Transactions of the American Institute of Electrical Engineers, Part II: Applications and Industry*, vol. 77, no. 1, pp. 41–42, 1958.
- [24] F. Savenije and J. Peeringa, “Control development for floating wind,” in *Journal of Physics: Conference Series*, vol. 524, Institute of Physics Publishing, 2014.
- [25] S. Christiansen, T. Bak, and T. Knudsen, “Minimum thrust load control for floating wind turbine,” in *Proceedings of the IEEE International Conference on Control Applications*, pp. 587–592, 2012.

-
- [26] F. Lemmer, S. Raach, D. Schlipf, and P. W. Cheng, "Prospects of linear model predictive control on a 10MW floating wind turbine," in *Proceedings of the International Conference on Offshore Mechanics and Arctic Engineering - OMAE*, vol. 9, American Society of Mechanical Engineers (ASME), 2015.
- [27] A. Kumar, P. Rainey, and E. Bossanyi, "LIDAR Assisted Model Predictive Control of a Next Generation Wind Turbine for Tower Fatigue Load Reduction and Improved Speed Control," 1 2015.
- [28] E. Simley, L. Pao, N. Kelley, B. Jonkman, and R. Frehlich, "LIDAR Wind Speed Measurements of Evolving Wind Fields," in *50th AIAA Aerospace Sciences Meeting Including the New Horizons Forum and Aerospace Exposition*, 1 2012.
- [29] A. Grauers, "Efficiency of three wind energy generator systems," *IEEE Transactions on Energy Conversion*, vol. 11, no. 3, pp. 650–655, 1996.
- [30] J. G. Njiri and D. Söffker, "State-of-the-art in wind turbine control: Trends and challenges," 2016.
- [31] W. E. Leithead, D. Leith, F. Hardan, and H. Markou, "Global gain-scheduling control for variable speed wind turbines," *EWECE 99*, 1999.
- [32] E. A. Bossanyi, "Wind Turbine Control for Load Reduction," *Wind Energy*, vol. 6, pp. 229–244, 7 2003.
- [33] B. Snyder and M. J. Kaiser, "Ecological and economic cost-benefit analysis of offshore wind energy," *Renewable Energy*, vol. 34, pp. 1567–1578, 6 2009.
- [34] B. Skaare, F. G. Nielsen, T. D. Hanson, R. Yttervik, O. Havmøller, and A. Rekdal, "Analysis of measurements and simulations from the Hywind Demo floating wind turbine," *Wind Energy*, vol. 18, pp. 1105–1122, 6 2015.
- [35] equinor.com, "World's first floating wind farm has started production."
- [36] Øyvind Gravås, "Hywind Scotland 5 turbines at Buchan Deep," 2017.
- [37] W. Leithead and S. Dominguez, "Coordinated control design for wind turbine control systems," 3 2006.
- [38] J. B. Hoagg and D. S. Bernstein, "Nonminimum-Phase Zeros," *IEEE Control Systems*, vol. 27, pp. 45–57, 6 2007.
- [39] C. Bak, F. Zahle, R. Bitsche, T. Kim, A. Yde, L. C. Henriksen, M. H. Hansen, J. P. A. A. Blasques, M. Gaunaa, and A. Natarajan, "The DTU 10-MW reference wind turbine," in *Danish Wind Power Research 2013*, 2013.
- [40] F. Lemmer, F. Amann, S. Raach, and D. Schlipf, "Definition of the SWE-TripleSpar floating platform for the DTU 10MW reference wind turbine," *University of Stuttgart*, 2016.
- [41] A. Fontanella, "Numerical model of a floating wind turbine controller and experimental implementation," 2017.

- [42] I. Horowitz and P. Rosenbaum, “Non-linear design for cost of feedback reduction in systems with large parameter uncertainty,” *International Journal of Control*, 1975.
- [43] H. Hu, Y. Zheng, Y. Chait, and C. Hollot, “On the zero-input stability of control systems with Clegg integrators,” in *Proceedings of the 1997 American Control Conference (Cat. No.97CH36041)*, pp. 408–410, IEEE, 1997.
- [44] O. Beker, C. Hollot, and Y. Chait, “Plant with integrator: an example of reset control overcoming limitations of linear feedback,” *IEEE Transactions on Automatic Control*, vol. 46, no. 11, pp. 1797–1799, 2001.
- [45] A. Barreiro, A. Baños, S. Dormido, and J. A. González-Prieto, “Reset control systems with reset band: Well-posedness, limit cycles and stability analysis,” *Systems and Control Letters*, 2014.
- [46] O. Beker, C. Hollot, and Y. Chait, “Stability of limit-cycles in reset control systems,” in *Proceedings of the 2001 American Control Conference. (Cat. No.01CH37148)*, pp. 4681–4682, IEEE, 2001.
- [47] L. Hazeleger, M. Heertjes, and H. Nijmeijer, “Second-order reset elements for stage control design,” in *2016 American Control Conference (ACC)*, pp. 2643–2648, IEEE, 7 2016.
- [48] L. Zaccarian, D. Nesic, and A. R. Teel, “Set-point stabilization of SISO linear systems using First Order Reset Elements,” in *2007 American Control Conference*, pp. 5808–5809, IEEE, 7 2007.
- [49] Y. Guo, Y. Wang, L. Xie, and J. Zheng, “Stability analysis and design of reset systems: Theory and an application,” *Automatica*, 2009.
- [50] D. Nešić, L. Zaccarian, and A. R. Teel, “Stability properties of reset systems,” in *IFAC Proceedings Volumes (IFAC-PapersOnline)*, 2005.
- [51] S. H. HosseinNia, I. Tejado, D. Torres, B. M. Vinagre, and V. Feliu, “A General Form for Reset Control Including Fractional Order Dynamics,” *IFAC Proceedings Volumes*, vol. 47, pp. 2028–2033, 1 2014.
- [52] M. Ivens, “Robust Reset Control using Adaptive / Iterative Learning Control,” 2018.
- [53] M. H. Hansen and L. C. Henriksen, “Basic DTU Wind Energy controller,” tech. rep., 2013.
- [54] A. D. Wright and L. J. Fingersh, “Advanced control design for wind turbines; Part I: control design, implementation, and initial tests,” tech. rep., National Renewable Energy Lab.(NREL), Golden, CO (United States), 2008.
- [55] R. M. Schmidt, G. Schitter, A. Rankers, and J. van Eijk, *The design of high performance mechatronics: High-tech functionality by multidisciplinary system integration: 2nd revised edition*. IOS Press, 1 2014.
- [56] I. E. Commission and others, “IEC 61400-1: Wind Turbines—Part 1: Design Requirements,” 2005.

- [57] K. Heinen, “Frequency analysis of reset systems containing a Clegg integrator: An introduction to higher order sinusoidal input describing functions,” 2018.

Glossary

List of Acronyms

FWT	floating wind turbine
FWT	Floating wind turbine
TSR	tip speed ratio
SWE	Stuttgart Wind Energy
DTU	Technical University of Denmark
RHP	right half-plane
FORE	first-order reset element
CI	Clegg integrator
DTU	Technical University of Denmark
SWE	Stuttgart Wind Energy
FAST	Fatigue, Aerodynamics, Structures, and Turbulence
MPC	model predictive controller
LIDAR	Light Detection and Ranging
SLOW	simplified low order wind turbine
MIMO	multiple input multiple output
SISO	single input single output
CgLp	constant gain, lead in phase
RHPZ	right half-plane zero
NTM	Normal Turbulence Model

RMS	root mean square
HOSIDF	higher-order sinusoidal input describing function
SORE	second-order reset element